INORGANIC CHEMISTRY
FRONTIERS

REVIEW

View Article Online
View Journal | View Issue

Check for updates

Cite this: *Inorg. Chem. Front.*, 2020, **7**, 2107

Correlation between crystal structures and polar (ferroelectric) properties of hybrids of haloantimonates(III) and halobismuthates(III)

R. Jakubas, M. Rok, K. Mencel, G. Bator and A. Piecha-Bisiorek *

Received 2nd March 2020,
Accepted 2nd April 2020

DOI: 10.1039/d0qi00265h

rsc.li/frontiers-inorganic

Halogenoantimonates(III) and halogenobismuthates(III) are a highly versatile class of organic–inorganic hybrid materials, applicable in optoelectronics and switchable dielectric devices. In this review, we discuss the rich chemistry of molecular–ionic halide complexes of Bi(III) and Sb(III) focusing on the correlations between their crystal structures and ferroelectric properties as well as on an explanation of the molecular mechanism of the paraelectric–ferroelectric phase transition. This review summarizes the current state of the art in the field of ferroelectricity among organic–inorganic hybrids based on Bi(III) and Sb(III) halides, which has become one of the key exploration areas of modern materials chemistry.

Published on 07 April 2020. Downloaded on 1/28/2026 4:44:51 PM.

1. Introduction

Materials whose physical properties can be controlled by external stimuli have attracted considerable interest due to their potential applications in substrate-film interfaces,[1–3] high-strain states, electrocaloric circuits,[4,5] nanotubes and nanowires,[6] ferroelectric random access memories (FeRAMs),[7] dynamic random access memory (DRAM) capacitors,[8–10] electron emitters,[2,8] solar cell components,[11] and weak-magnetic field sensors.[12–16] Ferroelectrics are of importance in the design of thermo-sensitive multifunctional switching materials because they are often accompanied by multiple switchable physical properties, *e.g.* piezoelectricity, pyroelectricity, dielectric constant and second harmonic generation (SHG). Ferroelectrics are polar substances in the solid state (crystalline or polymeric) or liquid-crystalline state (liquid crystals), in which a spontaneous polarization (P_s) is generated and it is reversible in an external electric field (E). The relationship between an electric shift (D) or polarization (P) and the electric field intensity leads to a hysteresis loop (D–E loop) between the opposite polarities. Such an electrical bistability can be used in non-volatile memory parts. It refers in particular to the ferroelectric computer memory type, FeRAM, which is crucial for

Faculty of Chemistry University of Wrocław, F. Joliot-Curie 14, 50-383 Wrocław, Poland. E-mail: anna.piecha@chem.uni.wroc.pl

Ryszard Jakubas

Ryszard Jakubas was born in 1951 in Ząbkowice Śl, Poland. He received his Ph.D. in 1980 from the University of Wrocław (Physics and Chemistry Faculty). He has been a professor at the Chemistry Department at Wrocław University since 1998. In 1991 he took scientific internship at Université de Lille Sciences et Technologies, France. In 2009, he was appointed as the head of the Physical Chemistry Department (University of Wrocław). He is the co-author of about 350 original scientific articles in the field of physicochemistry of organic–inorganic hybrid materials.

Magdalena Rok

Magdalena Rok was born in 1977 in Brzeg Dolny, Poland. She is an adjunct at the Faculty of Chemistry of the University of Wrocław. She obtained her Ph.D. in 2006 from the University of Wrocław. She took scientific internships at the Jülich Center for Neutron Science JCNS (MLZ, Garching, Germany), where she conducted research on neutron scattering in molecular complexes. Her current research interest is in functional metal complexes and coordination polymers based on their structural phase transitions. She is a member of the Ferroelectric and Liquid Crystals Team.

Published on 07 April 2020. Downloaded on 1/28/2026 4:44:51 PM.

Table 1 68 ferroelectric space groups belonging to the 10 polar point groups[17]

Crystal system	Polar point group		Space group	
Triclinic	1		*P*1	
Monoclinic	2	***m***	*P*2, *P*2$_1$, *C*2	***Pm*, *Pc*, *Cm*, *Cc***
Orthorhombic	*mm*2		*Pmm*2, *Pmc*2$_1$, *Pcc*2, *Pma*2, *Pca*2$_1$, *Pnc*2, *Pmn*2$_1$, *Pba*2, *Pna*2$_1$, *Pnn*2, *Cmm*2, *Cmc*2$_1$, *Ccc*2, *Amm*2, *Abm*2, *Ama*2, *Aba*2, *Fmm*2, *Fdd*2, *Imm*2, *Iba*2, *Ima*2	
Tetragonal	4	***4mm***	*P*4, *P*4$_1$, *P*4$_2$, *P*4$_3$, *I*4, *I*4$_1$	***P4mm*, *P4bm*, *P4$_2$cm*, *P4$_2$nm*, *P4cc*, *P4nc*, *P4$_2$mc*, *P4$_2$bc*, *I4mm*, *I4cm*, *I4$_1$md*, *I4$_1$cd***
Trigonal	3	***3m***	*P*3, *P*3$_1$, *P*3$_2$, *R*3,	***P3m*1, *P*31*m*, *P*31*c*, *P*3*c*1, *R*3*m*, *R*3*c***
Hexagonal	6	***6mm***	*P*6, *P*6$_1$, *P*6$_5$, *P*6$_2$, *P*6$_4$, *P*6$_3$	***P6mm*, *P6cc*, *P6$_3$cm*, *P6$_3$mc***

the application of novel materials. In principle all ferroelectrics have a Curie temperature, T_c, connected with the phase changes from the ferroelectric to paraelectric phase but some of them decompose before achieving T_c. When the temperature approaches T_c, the dielectric constant fulfilling the Curie–Weiss law undergoes an abnormal increase; this is a quantity, which can be used in capacitors. Pyroelectricity is another important quantity. The change of the P_s with temperature, when the crystal is being heated or cooled down, generates electric current. The pyroelectric effect is particularly enhanced just below the T_c temperature and is used in temperature sensors and in detecting infrared radiation. With regard to ferroelectrics, they comprise, for instance, coupled electrical and mechanical phenomena. The stress generates electric polarization charge known as the piezoelectric effect, and the electric field generates stress (electrostatics). Large piezoelectric and electrostriction effects are used in various types of devices, *e.g.* piezoelectric elements and microsensors. In addition, polar structures are the source of second order optical nonlinearity, which affects SHG and the linear electro-optical effect (Pockels Effect).

A considerable effort has been made so far to understand the switchable molecular dynamics of polar organic cations confined in various polymeric coordination hosts. However, due to the lack of in-depth knowledge on the relationship between the phase transition (PT) and crystal structure, a rational design of molecular ferroelectrics still represents a great challenge, especially of hybrid molecular–ionic ferroelectrics based on polar organic cations embedded in inorganic networks. The general symmetry consideration of almost all physical phenomena is a very effective way for obtaining their description. Ferroelectricity is no exception. From this point of view, there are 230 space groups and 32 point groups, which describe both the macro- and microscopic symmetries of crystal structures. Among the 32 point groups, 11 belong to the centrosymmetric classes, while the remaining 21 are noncentrosymmetric.[17] One should note, that the lack of spatial-inversion symmetry observed in the noncentrosymmetric group of crystals is most sought for in applications. It is important for the ferroelectric phase to adopt one of the 10 polar point groups, from which 68 polar space groups are formed (see Table 1).

The most important functionalities that make ferroelectrics so useful are the high values of the real part of complex dielectric permittivity, ε^*, spontaneous polarization, P_s, good mechanical and thermal resistance and small dielectric losses.[18,19] This set of traits determines the transition from the

Klaudia Mencel

Klaudia Mencel was born in 1992 in Ostrów Wielkopolski, Poland. She received her M.Sc. degree at the Faculty of Chemistry of the University of Wrocław in 2016. She is a Ph.D. student in the Ferroelectrics and Liquid Crystals Team, Faculty of Chemistry (University of Wrocław).

Grażyna Bator

Grażyna Bator was born in 1958 in Pleszew, Poland. She completed her Ph.D. in 1986 at the Faculty of Chemistry of the University of Wrocław, Poland. After presenting her habilitation dissertation in 2000, she obtained the title of Professor in 2007. She took scientific internships at KU Leuven in Belgium and ZIBJ in Dubna, FR, and carried out experiments on neutron scattering in cooperation with FRM II, Garching, Germany. She is the co-author of about 160 articles in the field of materials chemistry. She is the head of the specialization 'Materials Chemistry for Modern Technologies' at the Faculty of Chemistry of the University of Wrocław.

This journal is © the Partner Organisations 2020

Published on 07 April 2020. Downloaded on 1/28/2026 4:44:51 PM.

paraelectric phase (which is usually high-temperature, high symmetry state) to the ferroelectric one (low-temperature, low-symmetry state) in the close vicinity of the Curie temperature (T_c). The paraelectric–ferroelectric PT is related to the symmetry change (*e.g.* some symmetry elements of the paraelectric phase are lost, when the ferroelectric phase is reached), and leads to the structurally modified (ordered) ferroelectric phase. This structural transformation (described often as symmetry-breaking), is reflected in the macroscopic properties of the material, *e.g.* the appearance of P_s in the ferroelectric phases.

One of the classes of molecular–ionic materials are organic–inorganic hybrid ferroelectrics which are currently of particular interest, due to the designable and modifiable characteristics of their organic and inorganic components, for exploring ferroelectric-based multifunctional materials such as multiferroics, semiconductors and photovoltaic materials.[20–23] Of note, the symmetry, size, and value of the dipole moment and finally, the reorientations of the organic cations play an important role in triggering the structural PT. Therefore, control of the 'order–disorder' motion of the organic counterions in a molecular crystal is a key issue for the design of hybrid molecular–ionic ferroelectrics.

Haloantimonates(III) and halobismuthates(III), which are the subject of the present review, defined by the general formula $R_aM_bX_{3b+a}$, (where R – organic cations, M = Sb(III) or Bi(III) and X = Cl, Br, I) create one of the well-recognizable groups of ferroic compounds, essential mainly from an application point of view as they combine many desirable features, *e.g.* facile synthesis and processing, and cost-effectiveness with promising electrical and optical properties.[24–29] A characteristic feature of the compounds under consideration is that they possess the lone electron pair ($5s^2$ (Sb) and $6s^2$ (Bi)). However, its presence, which has a moderate impact on the structural properties of these salts, seems to have a tremendous effect on the physical properties of crystals. The lone electron pair deforms very easily a spherical symmetry of the orbital, on which they are located. This leads to an increase in the length of the M–X bonds, and thus to a considerable deformation of the MX_6 octahedra.

Anna Piecha-Bisiorek

Anna Piecha-Bisiorek was born in 1979 in Rybnik, Poland. She received her Ph.D. degree (supervisor: Prof. R. Jakubas) at the Faculty of Chemistry of the University of Wrocław in 2008 and became an assistant professor in 2018. She took scientific internships at the Jülich Center for Neutron Science JCNS (MLZ, Garching, Germany). Her research interests cover mainly the physicochemistry of organic–inorganic hybrid materials.

The polyanionic structure of the lattice is determined by the size of the organic cation, its symmetry and ability to create hydrogen bonds of the N–H···X type; the size of the halogen atom, which jointly creates the lattice is also of crucial importance. The alkylammonium cations belong to a wide variety of organic cations, which crystallize with various anionic sublayers. They are characterized by the different chain lengths, from methyl- to butyl-ammonium, and they may form five- or six-membered rings in the aromatic cations (*e.g.* imidazolium, pyridinium and its substituted derivatives) as well as saturated heterocyclic amines (*e.g.* pyrrolidine) (Fig. 1).

An analysis of these compounds has revealed a richness of the cationic unit movements. The motions depend on three basic factors such as: (i) the symmetry of the cation; (ii) the value of the dipole moments of the cation; (iii) the structure of the anionic network surrounding the cation. The reorientation ability of the dipolar units occupying vacancies inside the anionic sublayers is determined mainly by the symmetry and size of these spatial vacancies (a reorientational disorder), while the dynamic properties of the anionic networks are limited primarily by the formation of polymeric structures. In the organic part, the dynamic properties change significantly when the temperature is being lowered since the cation mobility decreases. This process is accompanied by a significant distortion of the anionic lattice. It must be mentioned that one of the most significant features of this lattice is its flexibility and, at the same time, its facility of adaptability of symmetric cations, which is related to the effect of the electron lone pair on the Sb(III) and Bi(III) atoms. The presence of hydrogen bonds of the N–H···X-type in the crystal structure is significant for the lattice formation. The strength of these bonds increases proportionally to the size of atom radius of the corresponding halogen. A rearrangement of these bonds takes place during the PT, which significantly affects the dynamic properties as well as the ordering of the cations.

In the present paper, we would like to focus on the ferroelectric structures among halogenoantimonates(III) and halogenobismuthates(III), which can be found in the literature and on the correlation between their crystal structures and polar properties. For this reason, the structural analysis of the compounds with the organic cations, a description of the cationic dynamics and the deformation of the inorganic layers have been undertaken. Moreover, macroscopic dielectric properties are discussed in detail.

2. Structural diversity of the anionic networks of haloantimonates(III) and halobismuthates(III)

Haloantimonates(III) and halobismuthates(III) are characterized by a significant diversity of the anionic networks (from zero-, through one-, two-, and three-dimensional architectures).[30–44] Taking into account the molar ratio of the amine (R) and metal (M) (Sb(III)/Bi(III)) the following four basic stoichiometries are observed.

Published on 07 April 2020. Downloaded on 1/28/2026 4:44:51 PM.

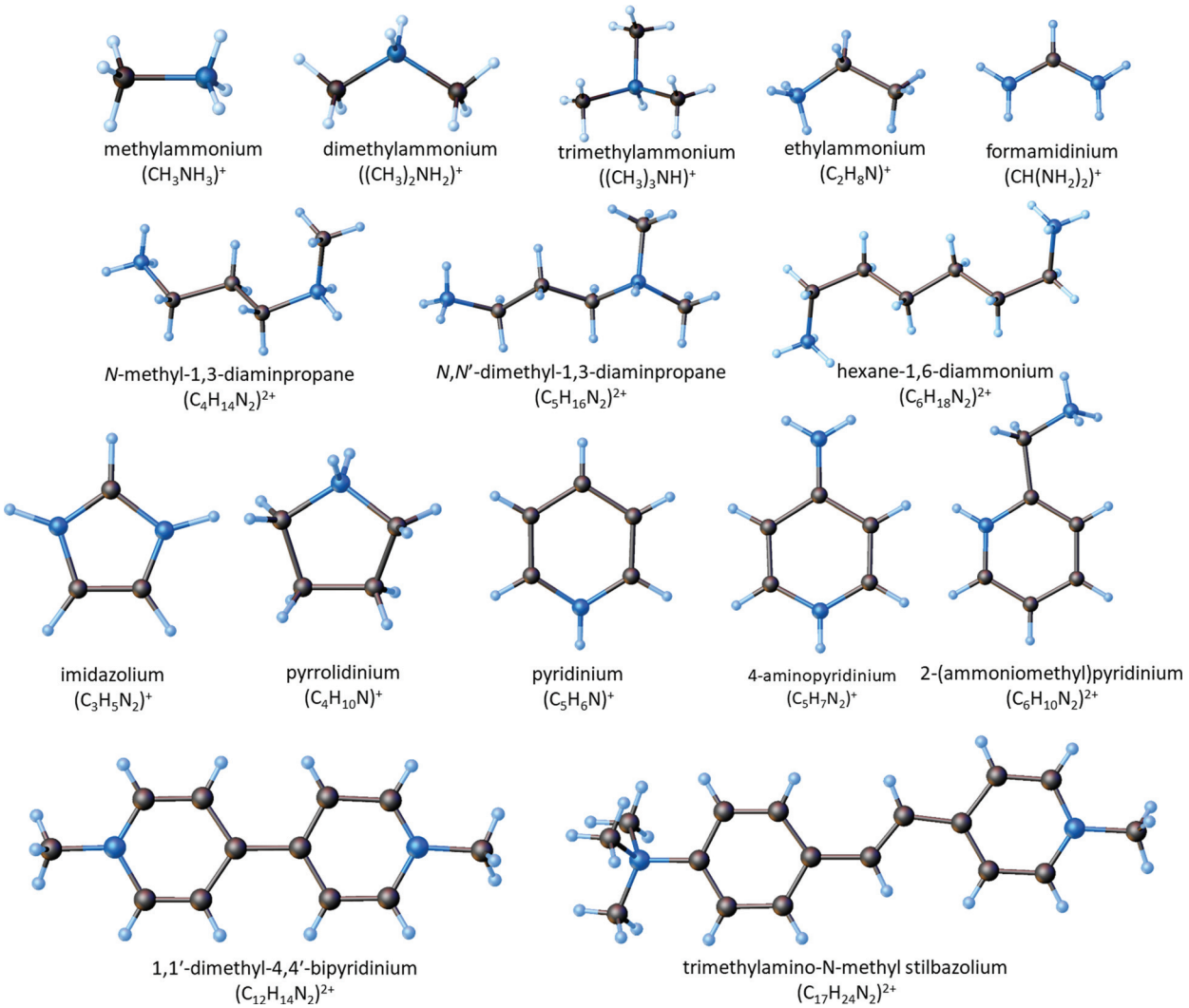

Fig. 1 Molecular structure of the organic cations creating ferroelectric compounds among halobismuthates(III) and haloantimonates(III).

2.1. RMX_4 (R : M = 1 : 1)

The anionic sublattices observed in this group may be divided into two types: (i) polyanionic chains; (ii) isolated units.

As for type (i) three different types of polyanionic chain arrangements are observed:

- chains of the edge-sharing octahedra (with two terminal and four bridging halogen atoms) (Fig. 2(a))[45–54]
- the $[MX_6]^{3-}$ octahedra linked as follows: three non-equivalent M atoms possess three bridging and three terminal contacts, whereas the remaining one possesses only one terminal and five bridging contacts (Fig. 2(b));[55]
- chains of the corner-sharing square pyramids (Fig. 2(c));[56]

With regard to the separated units (ii) four different assemblies may be recognized.

Four octahedra linked with each other in two different ways:

- one type of central atom with three bridging and three terminal halogens (Fig. 2(d))[57]
- two central atoms surrounded by three terminal and three bridging halogens and two others coordinated by two terminal and four bridging halogens (Fig. 2(e));[58–60]
- face-sharing octahedra (Fig. 2(f));[61,62]
- edge-sharing two square pyramids (Fig. 2(g));[63–70]

2.2. $R_3M_2X_9$ (R : M = 1.5 : 1)

•. infinite, one-dimensional (1D) *zig-zag* double chains (pleated ribbon structures) (Fig. 3(a));[71–76]

•. two-dimensional (2D) layers (honey-comb like corrugated sheets) (Fig. 3(b));[72,77–89]

•. discrete bioctahedra (0D) (Fig. 3(c));[45,90–94]

•. four octahedral units (0D) ($[M_4X_{18}]^{6-}$) (Fig. 3(d)).[95–99]

2.3. R_2MX_5 (R : M = 2 : 1)

- one-dimensional (1D) chains (*cis*- or *trans*-type) (Fig. 4(a) and (b) respectively)[100–109]
- isolated $[M_2X_{10}]^{4-}$ units (two edge-sharing octahedra) (Fig. 4(c));[49,110,111]

This journal is © the Partner Organisations 2020

Published on 07 April 2020. Downloaded on 1/28/2026 4:44:51 PM.

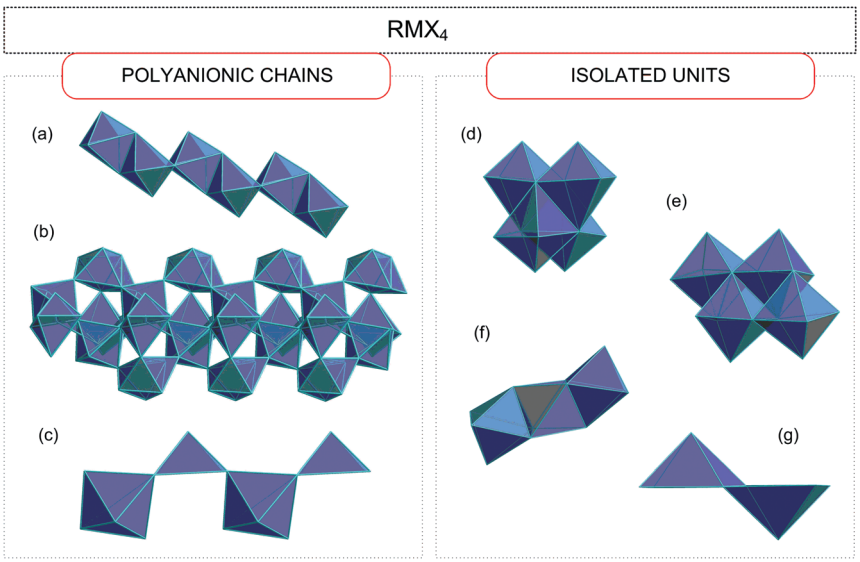

Fig. 2 Structures of anionic lattices with $[MX_4]^-$ stoichiometry: (a) infinite chain with edge-sharing octahedra; (b) infinite tape of differently joined octahedra; (c) infinite chain of square pyramids; (d) four octahedra possessing three bridging and three terminal halogens; (e) two octahedra with three terminal and three bridging halogens and two others with two terminal and four bridging halogens; (f) three face-sharing octahedra; (g) two edge-sharing pyramids.

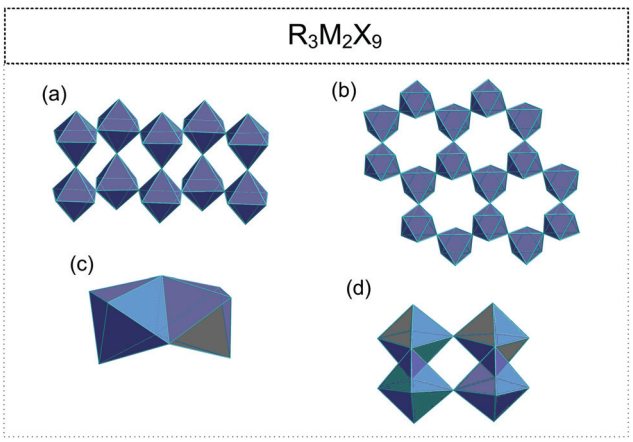

Fig. 3 Anionic structure of the $[M_2X_9]^{3-}$ composition; (a) one-dimensional double chain; (b) two-dimensional corrugated sheet; (c) two face-sharing octahedra; (d) four edge and corner-sharing octahedra.

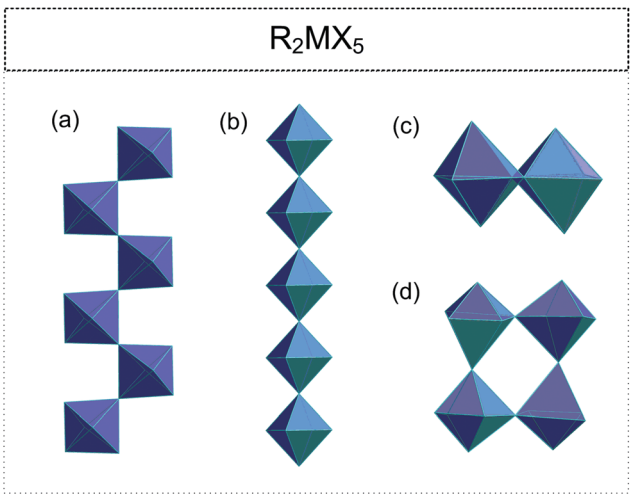

Fig. 4 Anionic structure of the $[MX_5]^{2-}$ composition; (a and b) the polyanionic chains with corner-sharing octahedra ((a) *cis*- (b) *trans*-configuration); (c) two edge-sharing octahedra; (d) a squaric structure containing four corner-sharing octahedra.

• tetrameric polyanion with corner-sharing octahedra (Fig. 4(d)).[55,112]

2.4. $R_5M_2X_{11}$ (R : M = 2.5 : 1)

• Corner-sharing octahedra (0D) ($[M_2X_{11}]^{5-}$) (Fig. 5(a)).[113–123]

2.5. R_3MX_6 (R : M = 3 : 1)

• Isolated $[MX_6]^{3-}$ octahedra (Fig. 5(b)).[124–133,134,135]

2.6. Different modifications of the anionic substructures

The richness of the anionic structures among halobismuthates(III) and haloantimonates(III) is related also to the more exotic type of stoichiometry[34,136] (see Fig. 6), *e.g.* RM_2X_7,[137,138] RM_3X_{10},[139–141] $R_3M_5X_{18}$,[99,142,143] $R_4M_6X_{22}$,[142–144] $R_4M_8X_{28}$[138,139] or $R_6M_8X_{30}$.[145]

3. Ferroelectricity among haloantimonates(III) and halobismuthates(III)

The ferroelectricity among halobismuthates(III) and haloantimonates(III) is limited only to four different types of chemical

Published on 07 April 2020. Downloaded on 1/28/2026 4:44:51 PM.

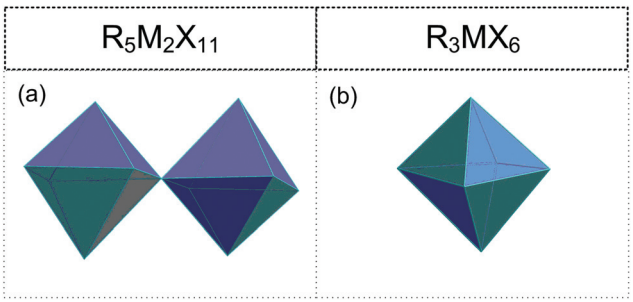

Fig. 5 (a) Structure of the isolated $[M_2X_{11}]^{5-}$ anions; (b) isolated $[MX_6]^{3-}$ octahedra.

compositions: RMX_4, $R_3M_2X_9$, R_2MX_5 and $R_5M_2X_{11}$. Below, the analysis of the physical properties is presented and a correlation between the crystal structure and the origin of their polarity (ferroelectricity) is discussed. In our review we focus on pure organic–inorganic hybrids based on Bi(III) and Sb(III) (mixed anionic networks were not analyzed); however, due to the discovery of the first ferroelectric among halobismuthates (III) characterized by the mixed organic networks ($R'R_2''MX_6$) a single exception has been made.

3.1. RMX_4 type compounds

Ferroelectricity in the RMX_4 type compounds is a unique feature. Based on the literature, only two examples of ferroelectrics, characterized by the 1D polymeric anionic structure, are known: (4-aminopyridinium)$[SbCl_4]$[51–53] ($(4\text{-}NH_2C_5H_4NH)[SbCl4]$, 4-APCA) and (trimethylamino-*N*-methyl stilbazolium) $[Bi_2Cl_8]$[54] ($(C_{17}H_{24}N_2)[Bi_2Cl_8]$, (TAMS)$[Bi_2Cl_8]$). The detailed X-ray structure analysis indicates that in both compounds, the ferroelectricity is related mainly to a strong deformation of the $[MX_4]^-_\infty$ type of substructure (see Fig. 2(a) and Table 2).

The crystal structure of 4-APCA is built up of the polyanionic chains of $[SbCl_4^-]_\infty$ forming a tunnel-like structure and disordered 4-aminopyridinium cations connected *via* weak hydrogen bonds. Phase situation is complex and characterized by rich polymorphism in the solid state (see Scheme 1). The ac calorimetry studies have shown that the high temperature PT at 304 K is of the 'order – disorder' type and leads to a incom-

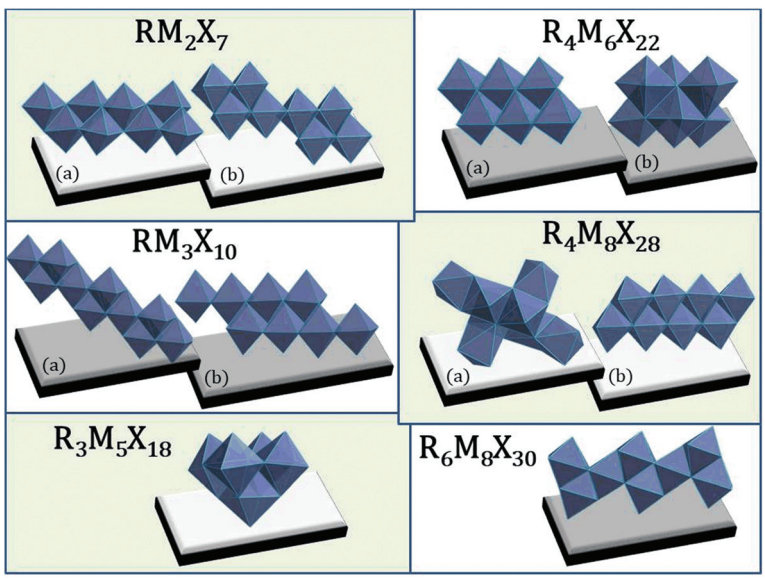

Fig. 6 Atypical anionic structures among haloantimonates(III) and halobismuthates(III). ((a and b) labels correspond to the different organization of the inorganic structures) RM_2X_7 polyanionic 1D chains; $R_4M_6X_{22}$ 0D units; RM_3X_{10} infinite (1D) polyoctahedral chains; $R_4M_8X_{28}$, $R_3M_5X_{18}$, $R_6M_8X_{30}$ isolated (0D) units.[137–145]

Table 2 Phase diagram of RMX_4 stoichiometry

		Ref.
$(4\text{-}NH_2C_5H_4NH)[SbCl_4]$	245 K, 1st: V: $P2_1/c$ | 250 K, 2nd: IV: Cc | 271 K, 2nd: III: Cc | 304 K,2nd: II: $C2/c$ | I: $C2/c$	51–53
	$P_s = 0.35\ \mu C/cm^2$, $\varepsilon_{max} \cong 700$	
$(C_{17}H_{24}N_2)[Bi_2Cl_8]$	I: $Pna2_1$	54
	$P_s = 0.08\ \mu C/cm^2$, $\varepsilon_{max} \cong 250$	

1st-first order PT, 2nd-second order PT ferroelectric phase paraelectric phase

 This journal is © the Partner Organisations 2020

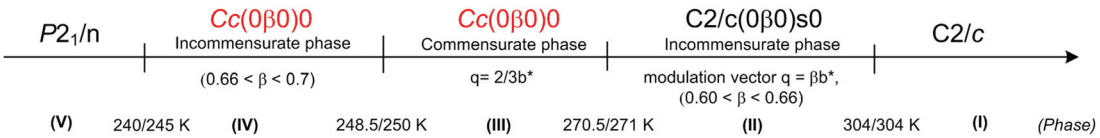

Scheme 1 Phase diagram of 4-APCA.[51–53]

mensurate modulated phase (II). At 270.5 K (II → III) a 'lock-in' transition to a commensurate modulated phase is observed, which, in turn, becomes a ferroelectric one. The anomaly at 248 K leads to the next polar, but modulated incommensurate phase, while below 240 K the crystal becomes nonpolar again. The ferroelectric transformation at 270.5 K is characterized by a 'displacive' type of mechanism related to the displacement of the organic cations in relation to the anionic chains. Dielectric dispersion measurements carried out in the radio-frequency region around T_c (270.5 K) revealed a critical slowing-down assigned mainly to the domain-like wall motion of the incommensurate phase (Fig. 7(a)). The relaxation process was found to be nearly monodispersive, which is rare among incommensurate ferroelectrics.[146] The polar properties of 4-APCA were confirmed by the switchable P_s of about 0.35 μC cm^{-2} at 265 K. One should note that among halogenobismuthates(III) and halogenoantimonates(III), 4-APCA was the first example of a ferroelectric compound characterized by the molecular mechanism of a 'displacive'-type assigned to the ferroelectric PT.

With regard to (TAMS)[Bi_2Cl_8], it belongs to room temperature (RT) ferroelectrics, but the Curie temperature was not achieved on heating due to the earlier decomposition of the compound. (TAMS)[Bi_2Cl_8] crystallizes in an acentric orthorhombic space group ($Pna2_1$) and consists of a framework of infinitive $[Bi_2Cl_8]^{2-}_{\infty}$ inorganic chains, separated by $[TAMS]^{2+}$ cations. The non-centrosymmetric crystal structure and polar alignment of the organic species contribute to the P_s value, which is of the order of 0.08 μC cm^{-2} at 453 K.

The dielectric measurements confirm the lack of PT in a wide temperature range and indicate the existence of the dielectric relation process (Fig. 7(b)). The expected effect of the slowing down of the macroscopic relaxation time, related to the dynamics of the ferroelectric domains, is not observed when approaching the *para*-ferroelectric transition, which might be connected to the huge contribution of the electric conductivity to the dielectric response. It should be noted that the estimated relaxation time for the relaxation process in (TAMS)[Bi_2Cl_8] becomes shorter on heating, which is a quite opposite effect in comparison with that observed in the other ferroelectrics. This is characteristic of the systems with dipolar group reorientations without any long-range dipole–dipole interactions. The activation energy of the relaxation process calculated from the Arrhenius relationship, E_a, equals to 280 kJ mol^{-1} and may be a result of some dipole cooperative motions or steric hindrance originating from the huge organic molecule as for the single dipole motion.[54]

3.2. $R_3M_2X_9$ type compounds

Within the chemical stoichiometry $R_3M_2X_9$ the ferroelectricity is limited to two types of anionic sublayers among four possible ones (Fig. 3); 2D (two-dimensional layers) (Fig. 3(b)) and 0D-discrete bioctahedral units (Fig. 3(c)). The 2D structure is usually characteristic of the chloride and bromide ferroelectrics containing only small alkylammonium moieties (methyl-, dimethyl and trimethyl-ammonium) or non-substituted rings (*e.g.* pyrrolidinium cation) (Table 3). The bulky organic cations due to the steric effects cannot occupy small vacancies within the layers. On the other hand all known iodide ferroelectrics possess the 0D anionic network (Table 4) thus the restriction with respect to the size and symmetry of the organic moieties is not so obvious.

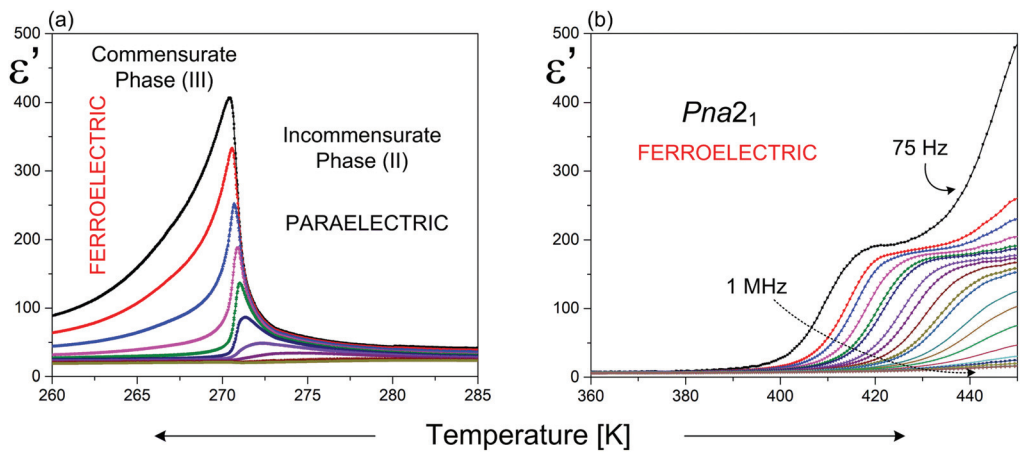

Fig. 7 Temperature dependence of the real part of the complex dielectric permittivity for: (a) 4-APCA;[51] (b) (TAMS)[Bi_2Cl_8].[54]

Published on 07 April 2020. Downloaded on 1/28/2026 4:44:51 PM.

Published on 07 April 2020. Downloaded on 1/28/2026 4:44:51 PM.

Table 3 Phase diagram of $R_3M_2X_9$ with a 2D anionic architecture

	Ref.
$(CH_3NH_3)_3[Bi_2Br_9]$ 	82, 84 and 85
$(CH_3NH_3)_3[Sb_2Br_9]$ 	81
$((CH_3)_2NH_2)_3[Sb_2Br_9]$ 	86 and 87
$((CH_3)_2NH_2)_3[Sb_2Cl_9]$ 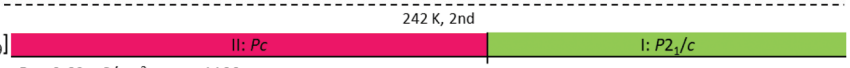	83 and 88
$((CH_3)_3NH)_3[Sb_2Cl_9]$ 	72, 78, 79, 83 and 89
$(C_4H_8NH_2)_3[Sb_2Cl_9]$ 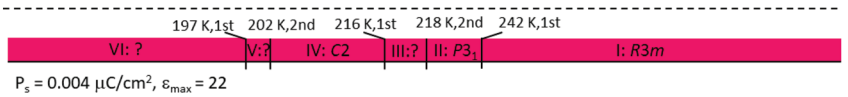	80

1st-first order PT, 2nd-second order PT ferroelectric phase paraelectric phase

The characteristic feature of the paraelectric phase in 2D $R_3M_2X_9$ ferroelectrics is the presence of two crystallographically independent alkylammonium cations in the crystal structure (N(1) and N(2)). The cation N(1) is located in voids inside the polyanionic layers, whereas the N(2) one between the layers (Fig. 8). All cations are connected to the anionic sublattice by N–H···X hydrogen bonds. Both types of cations are highly disordered in the paraelectric phase.

The disorder of N(1) is usually described by a two-site model with an occupancy factor of the N(1) atom, equal to 0.5. The other cation N(2) is also split between two positions, N(21) and N(22), however, with different occupancy factors, which change with temperature. Since the N(2) cation is in the general position of the crystal structure, this change does not lead to any changes in the lattice symmetry in contrast to the N(1) cation dynamics. The paraelectric–ferroelectric transitions lead to the distortion of the anionic network, which results in the loss of the symmetry center. Thus the N(1) cations now occupy a single position in a ferroelectric domain and their long-range order is responsible for an appearance of P_s. In the

Table 4 Phase diagram of $R_3M_2X_9$ with a 0D anionic architecture

	Ref.
$(CH_3NH_3)_3[Bi_2I_9]$ 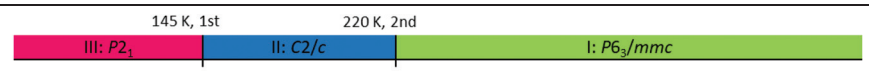	147 and 148
$(C_5H_{12}N)_3[Sb_2Br_9]$ 	149 and 150
$(C_5H_{12}N)_3[Sb_2Cl_9]$ 	149
$(NH_2CHNH_2)_3[Bi_2I_9]$ 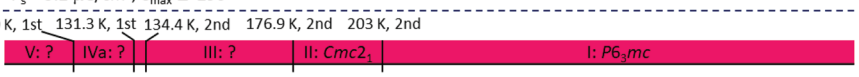	151
$(NH_2CHNH_2)_3[Sb_2I_9]$ 	152
$((CH_3)_3NH)_3[Bi_2I_9]$ 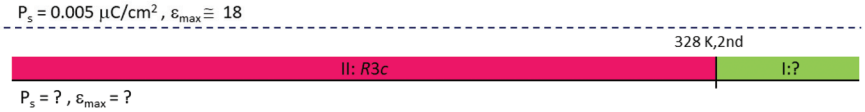	153

1st-first order PT, 2nd-second order PT ferroelectric phase paraelectric phase

 This journal is © the Partner Organisations 2020

Published on 07 April 2020. Downloaded on 1/28/2026 4:44:51 PM.

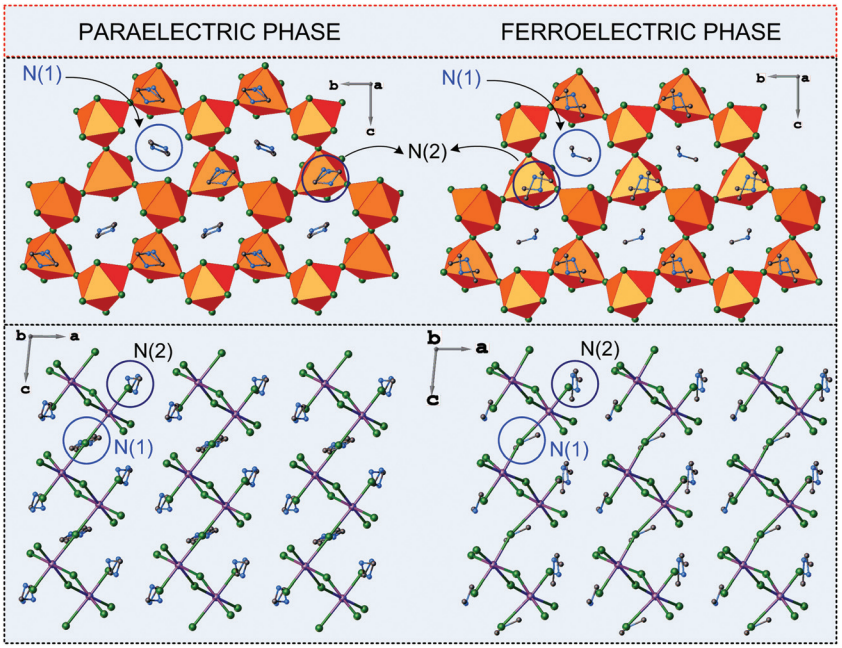

Fig. 8 Comparison of the crystal structures of DMACA in the paraelectric and ferroelectric phases (ref.88).

case of the 2D ferroelectrics the polar direction is maintained within the corrugated layer structure. This means that the layers enhanced the polarizability of the system, which is coupled with the dynamics of the N(1) type cations.

An enhanced value of the electric permittivity close to T_c is observed for the 2D ferroelectrics, because easily polarizable anionic layers favor the long-range order of the dipole–dipole interactions (Fig. 9).

In spite of the structural similarities of the 2D type ferroelectrics their dielectric responses, character of PTs and phase situations are quite diverse. The dielectric response of the majority of the 2D analogs shows a critical slowing down of the macroscopic relaxation time, which indicates an 'order–disorder' mechanism of ferroelectric transition (Fig. 9(a)). In turn in the case of MABB the dielectric response ($\varepsilon(T)$) is characteristic of 'improper' ferroelectrics (1st – order PT)

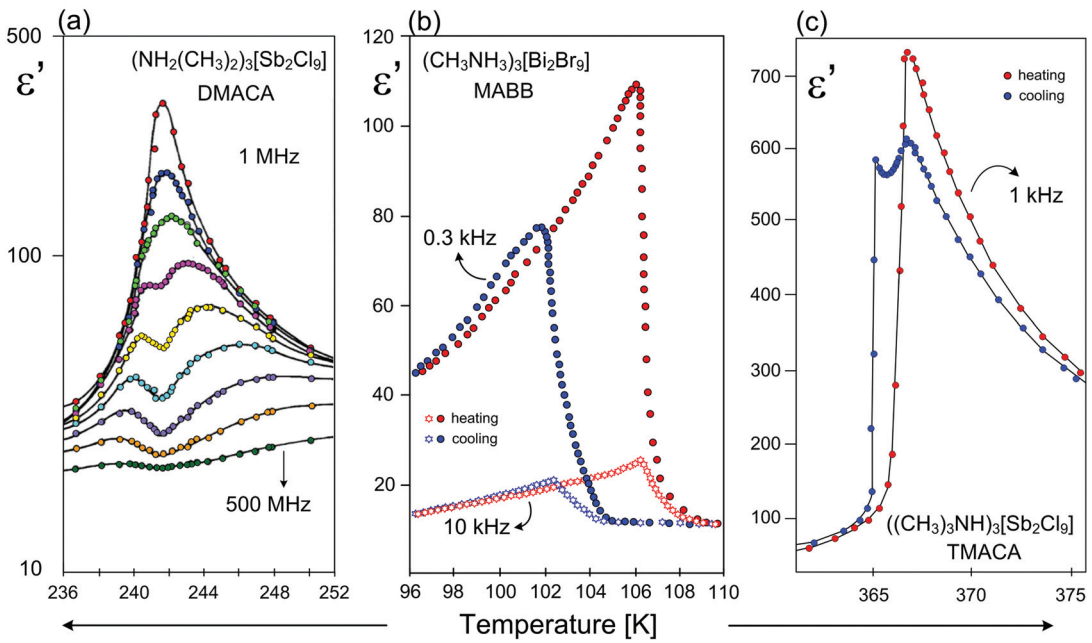

Fig. 9 Temperature dependence of the real part of the dielectric permittivity (ε') for (a) $((CH_3)_2NH_2)_3[Sb_2Cl_9]$ (DMACA)[131] (b) $(CH_3NH_3)_3[Bi_2Br_9]$ (MABB);[84,85] (c) $((CH_3)_3NH)_3[Sb_2Cl_9]$ (TMACA);[131] around T_c.

Published on 07 April 2020. Downloaded on 1/28/2026 4:44:51 PM.

(Fig. 9(b)), while for the TMACA the dielectric results indicate the existence of a narrow-range intermediate metastable phase (incommensurate) between the ferroelectric and paraelectric phases (Fig. 9(c)).

The only parameter that correlates well with the temperature scope of the ferroelectric phases is the cation size (Tables 3 and 4). It is clearly seen that an increase of the cations size leads to the shift of the Curie point towards high temperatures. The large cations usually have less freedom of movement in the anion layer (N(1)-type) gaps, which is why they are easier to freeze at higher temperatures in cooling cycles in comparison with the ferroelectrics with the small cations.

Haloantimonates(III) and halobismuthates(III), characterized by the 2D anionic structure, usually possess a smaller value of P_s in contrast to that for the 0D analogs, in spite of the fact that the organic cations of the presented crystals have a larger value of dipole moments, μ. Nevertheless it should be noted that in the formamidinium analogs the cations possess a quite small value of μ = 0.23 D and the dielectric anomalies are rather intermediate. It seems that the relationship between structural parameters of the crystals and the macroscopic properties (P_s and ε_{max}) is rather complex and its recognition requires further studies on $R_3M_2X_9$-type compounds. It is interesting that most 0D ferroelectrics possess polar properties above room temperature, except for $(NH_2CHNH_2)_3[Bi_2I_9]$[151] and $(NH_2CHNH_2)_3[Sb_2I_9]$.[152] The paraelectric phase exhibits usually high symmetry (trigonal or hexagonal), which proves a high dynamic disorder of the cationic networks. Generally, the mechanism of ferroelectric phase transitions for the 0D compounds is quite complex because the 'order–disorder' and 'displacive' contributions are possible.

3.3. R_2MX_5 type compounds

A Cambridge Structural Database survey (version 5.40 March 2019) permits us to predict the probability of the appearance of acentric/ferroelectric compounds within R_2MX_5-type stoichiometry. 192 entries, adopting either polymeric (1D) or isolated (0D) anionic substructures, have been found.

The results presented in Tables 5 and 6 confirm that the ferroelectricity in the R_2MX_5-type compounds is adopted in the 1D anionic network. The ferroelectricity does not depend on the symmetry and size of the organic cations (heteroaro-

Table 5 Phase diagram of R_2MX_5 or RMX_5 stoichiometry

		Ref.
$(C_{12}H_{14}N_2)[BiI_3Cl_2]$	I: $P2_1$ P_s > 15 μC/cm²	107
$(C_6H_{18}N_2)$ $[BiI_5]$	379 K, 1st II: $Pna2_1$ | I: $Pnma$ P_s = 6.2 μC/cm², $\varepsilon_{max} \cong$ 2400	154
$(NH_2(CH_2)_3NHCH_3)$ $[BiCl_5]$	376 K, 1st II: $Pna2_1$ | I: $Pnma$ P_s = 2.38 μC/cm², $\varepsilon_{max} \cong$ 40	155
$(C_6H_{10}N_2)$ $[SbI_5]$	360 K, 2nd 390 K, 1st III: $Pb2_1a$ | II: $Pbca$ | I: $Pbca$ P_s = 4 μC/cm², $\varepsilon_{max} \cong$ 18	156
$(C_4H_8NH_2)_2[BiCl_5]$	236 K, 1st 248 K, 1st 255 K, 2nd IV: Pn | III: $P1n1$ | II: $Pmn2_1$ | I: $Pmnb$ P_s = 0.4 μC/cm² (T<248 K), P_s = 0.16 μC/cm² (T<236 K), $\varepsilon_{max} \cong$ 50	100
$(C_{12}H_{14}N_2)[BiBr_5]$	243 K, 2nd II: $P2_1$ | II: $P2_1/c$ P_s = n/a, $\varepsilon_{max} \cong$ 300	157
$(C_2H_5NH_3)_2[BiCl_5]$	190 K, 1st II: $Aba2$ | I: $Acam$ P_s = 1.4 μC/cm², $\varepsilon_{max} \cong$ 20	102
$(C_3H_5N_2)_2[SbCl_5]$	180 K, 2nd 342 K, 1st III: $Pna2_1$ | II: $Pbcn$ | I: ? P_s = 0.8 μC/cm², $\varepsilon_{max} \cong$ 1200	158
$(C_2H_5NH_3)_2[BiBr_5]$	120 K, 2nd 160 K, 1st III: $Aea2$ | II: $Pca2_1$ | I: $Aeam$ P_s = 0.005 μC/cm², $\varepsilon_{max} \cong$ 55	159
$(C_5H_{16}N_2)[BiBr_5]$	143 K, 2nd II: Pc | I: $P2_1/c$ P_s = 1 μC/cm², $\varepsilon_{max} \cong$ 6300	160

1st-first order PT, 2nd-second order PT ferroelectric phase paraelectric phase

 This journal is © the Partner Organisations 2020

Published on 07 April 2020. Downloaded on 1/28/2026 4:44:51 PM.

Table 6 The results of CSD analysis

Anionic substructure	All compounds	Piezoelectric	Ferroelectric
Isolated pyramids $[MX_5]^{2-}$	35	8	0
Isolated bioctahedra $[M_4X_{10}]^{4-}$	81	2	0
Isolated tetrameric forms $[M_4X_{20}]^{8-}$	4	1	0
Infinite chains $[MX_5]_\infty$	72	30	9
Summary	**192**	**41**	**9**

matic, heterocyclic aliphatic) but is strongly affected by the dipole moment values.

A characteristic feature of this subclass is the construction of the anionic lattice, which is created by 1D infinite chains of different configurations (*cis*- or *trans*-mode), however, the *cis*-conformation (and its modifications) is very common in the analyzed subgroup. Generally, one can state that the distortion of the anionic chains through the PT is a driving force, which contributes mainly to the P_s value. This effect is coupled with the dynamics of the polar organic cations, which are usually disordered in the paraelectric phase to varying degrees. Distortion of the anionic substructure is treated as a 'displacive' contribution to the molecular mechanism of the ferroelectric transition, whereas a change in the dynamics of the organic moieties is an 'order–disorder' contribution (Fig. 10).

The molecular mechanism of the paraelectric-ferroelectric transformation varies from 'displacive' through mixed up to purely 'order–disorder', however, which of these mechanisms is dominant depends strongly on the subtle differences in the development of the polyanionic chains. In the case of the 'displacive' R_2MX_5 subclass we should take into account the ns^2 electron lone pair effect ($5s^2$-Sb and $6s^2$-Bi), which seems to play a key role in the distortion of the MX_6 octahedron. The derivatives, characterized by *trans*-connected octahedra containing bulky organic methylviologen MV^+ amine: (MV)$[BiBr_5]$,[157] (MV)$[BiI_3Cl_2]$, are an example of such a distorted structure.[107] The MV^{2+} cations have stabilized unprecedented regular $[BiBr_5^{2-}]_\infty$ chains of *trans*-connected octahedra.

Through PT, the trans Bi–Br bonds differentiate markedly and the result is the chain polarity. Moreover, the electronic lone pair is stereochemically activated below 243 K leading to an acentric polar phase. The mixed-halide analog, (MV)$[BiI_3Cl_2]$, reaches one of the highest room-temperature P_s values (>15 μC cm^{-2} at 298 K) in the field of organic–inorganic hybrid ferroelectrics. It should be added that *trans*-connected isomers are much rarer than *cis*-connected ones. It is difficult to indicate a different correlation between the crystal structure and dynamics and the scope of polar phases in this group of compounds.

Compared to $R_3M_2X_9$ connections, the organic cations in R_2MX_5 show less freedom of movement in the paraelectric phases (usually a two-site model) thus the compounds adopt

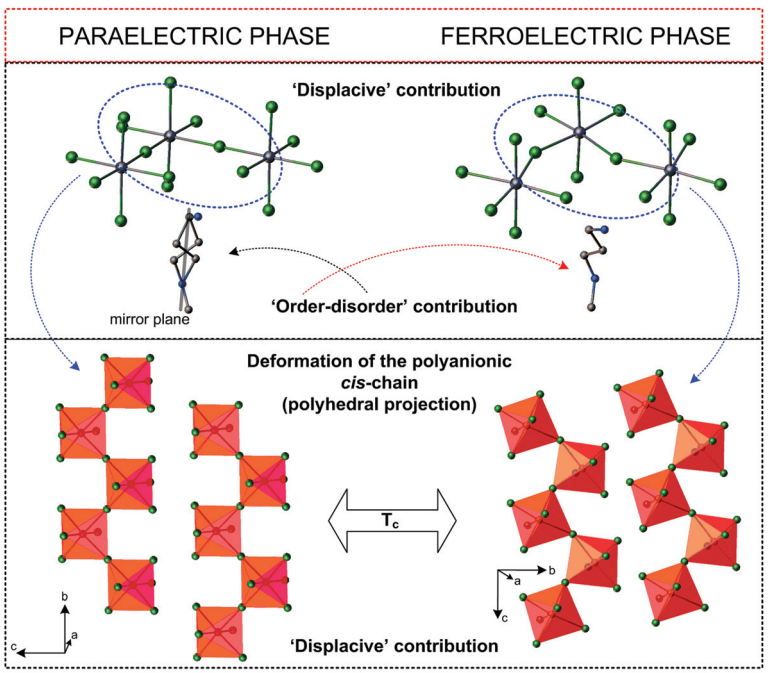

Fig. 10 Comparison of the crystal structures of $(NH_2(CH_2)_3NHCH_3)[BiCl_5]$[155] in the paraelectric and ferroelectric phases.

Published on 07 April 2020. Downloaded on 1/28/2026 4:44:51 PM.

lower symmetry (mainly orthorhombic). Thus most of the paraelectric-ferroelectric transitions in the R_2MX_5-subclass is described by the *mmmFmm*2 Aizu relationship (non ferroelastic transitions), in turn methylviologen analogs characterized by *trans*-connected-modes of the anionic chains exhibit also non-ferroelastic transition between monoclinic phases described by 2/*mFm* or 2/*mF*2 species (Fig. 11).

As it is presented (Table 5) for the hybrids based on very similar organic cations (*N*-methyl-1,3-diaminopropane) and (*N*,*N*-dimethyl-1,3-diaminopropane) the differences in the T_c values (existence of polar phases) reach about 230 K (376 and 143 K, respectively), however, the values of P_s are comparable (2.38 and 1.36 μC cm^{-2}, respectively). In turn, the organic–inorganic compounds based on the ethylammonium cation indicate similar values of T_c (190 and 160 K), while P_s differs almost by three orders 1.4 and 5 × 10^{-3} μC cm^{-2}. In conclusion, within R_2MX_5-type ferroelectrics the amount of the deformation of the anionic chains is crucial, when it comes to the value of P_s and a character of the dielectric response close to T_c (Fig. 12).

3.4. $R_5M_2X_{11}$ type compounds

Complexes of $R_5M_2X_{11}$ stoichiometry are unique in crystalochemistry of haloantimonates(III) and halobismuthates(III). Currently, scientific literature gives only seven examples of the compounds marked by this type of chemical composition and all of them exhibit ferroelectric properties (see Table 7). A typical trait of the compounds in question is the presence of

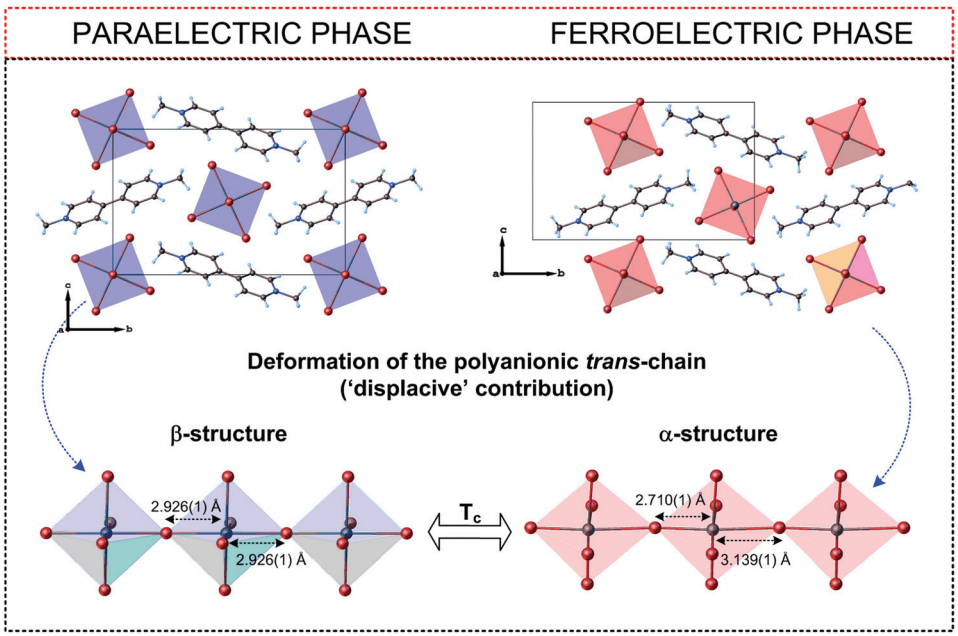

Fig. 11 Comparison of the crystal structures of $(C_{12}H_{14}N_2)[BiBr_5]$[157] in the paraelectric and ferroelectric phases.

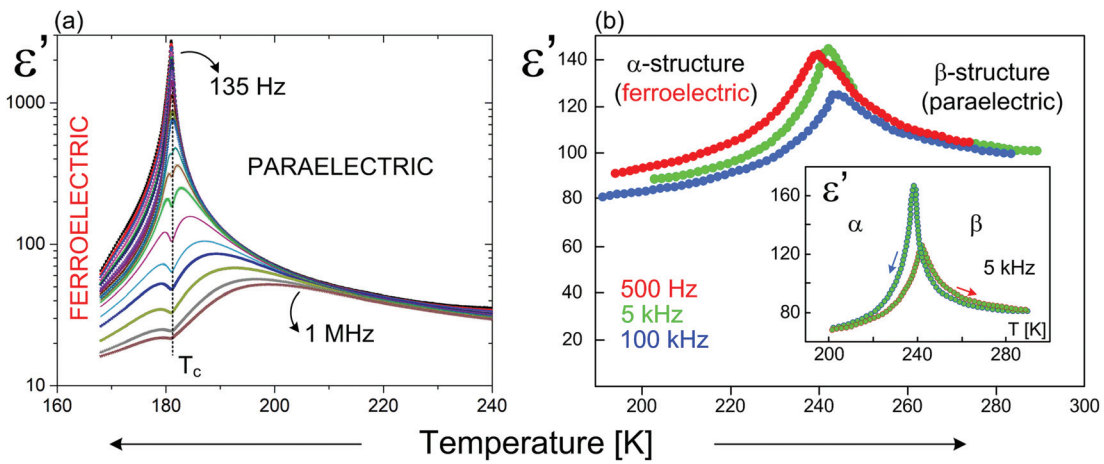

Fig. 12 Temperature dependence of the real part of the complex dielectric permittivity for: (a) $(C_3H_5N_2)_2[SbCl_5]$;[158] (b) $(C_{12}H_{14}N_2)[BiBr_5]$.[157]

This journal is © the Partner Organisations 2020

Published on 07 April 2020. Downloaded on 1/28/2026 4:44:51 PM.

Table 7 Phase diagram of $R_5M_2X_{11}$

		Ref.
$(CH_3NH_3)_5[Bi_2Br_{11}]$	77 K, 2nd; 312 K, 2nd III: $P2_1$ | II: $Pca2_1$ | I: $Pcab$ P_s = 0.86 μC/cm², $\varepsilon_{max} \cong$ 8000	116–118
$(CH_3NH_3)_5[Bi_2Cl_{11}]$	170 K, 2nd; 250 K, 2nd; 307 K, 2nd IV: $P2_1$ | III: $P2_1$ | III: $Pca2_1$ | I: $Pcab$ P_s = 2 μC/cm², $\varepsilon_{max} \cong$ 20000	119–122
$(NH_2CHNH_2)_5[Sb_2Br_{11}]$	163 K, 2nd; 200 K, 1st; 233 K, 2nd IV: $P2_1$ | III: $P2_1/n$ | II: $P2_1/n$ | I: $Pmnn$ P_s = 3 μC/cm², $\varepsilon_{max} \cong$ 55	163
$(C_3H_5N_2)_5[Bi_2Cl_{11}]$	166 K, 2nd; 360 K, 1st III: Pn | II: $P2_1/n$ | I: ? P_s = 0.6 μC/cm², $\varepsilon_{max} \cong$ 300	113
$(C_3H_5N_2)_5[Bi_2Br_{11}]$	155 K, 2nd; 355 K, 1st III: Pn | II: $P2_1/n$ | I: ? P_s = 0.3 μC/cm², $\varepsilon_{max} \cong$ 220	114
$(C_3H_5N_2)_5[Sb_2Br_{11}]$	135 K, 2nd; 145 K, 2nd; 354 K, 1st IV: Pn | III: Pn | II: $P2_1/n$ | I: ? P_s = 0.18 μC/cm², $\varepsilon_{max} \cong$ 250	123
$(C_5H_5NH)_5[Bi_2Br_{11}]$	118 K, 2nd; 405 K, 1st III: $P2_1$ | II: $P2_1/n$ | I: ? P_s = 0.3 μC/cm², $\varepsilon_{max} \cong$ 220	115

1st-first order PT, 2nd-second order PT ferroelectric phase paraelectric phase

discrete bioctahedral units, $[M_2X_{11}]^{5-}$ in their crystal structure, in which two octahedra are connected with each other by one bridging halogen atom (see Fig. 13).

A cationic subnetwork consists in turn of four kinds of nonequivalent types of organic species marked by varied dynamic disorder. Phase situation for all $R_5M_2X_{11}$-ferroelectrics is presented in Table 7.

A detailed analysis of the phase diagrams and structural data shows that the size of the organic cation and its shape and symmetry, have a significant influence on PTs' sequence, on the symmetry of each phase, on the polar properties of compounds as well as on the temperature range of the existence of the polar (ferroelectric) phases. Thus, this group may be divided into two subgroups: the first one created by the hybrids based on the aliphatic cations, *e.g.*: $(CH_3NH_3)_5[Bi_2Br_{11}]$,[116–118] $(CH_3NH_3)_5[Bi_2Cl_{11}]$[119–122] and $(NH_2CHNH_2)_5[Sb_2Br_{11}]$[163] (abbreviated as aliphatic analogs) and the second one formed by aromatic counterions:

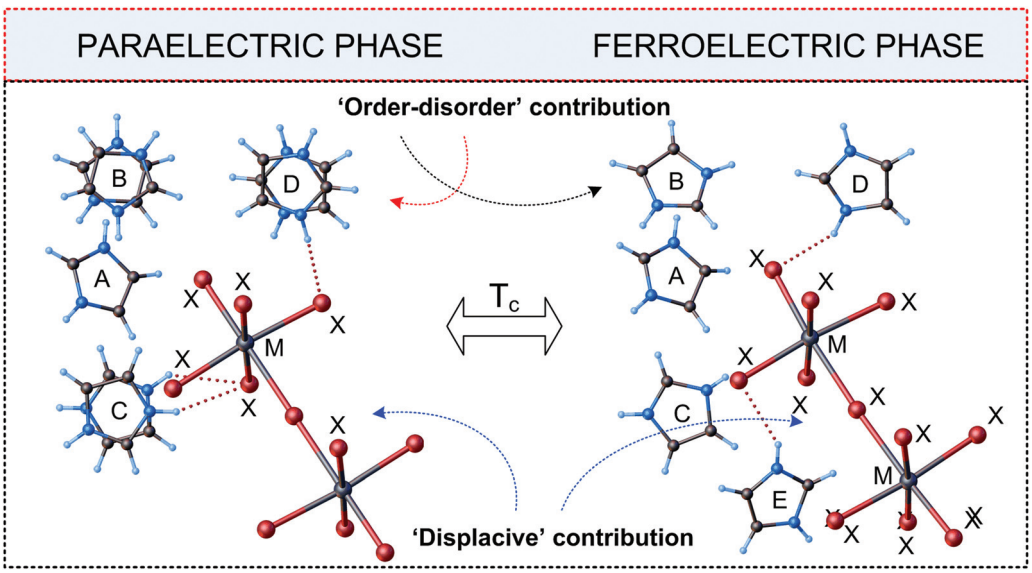

Fig. 13 Independent parts of the unit cell of $[C_3N_2H_5]_5[Bi_2Br_{11}]$ in the paraelectric and ferroelectric phases (M = Bi(III)/Sb(III), X = Cl, Br, I).[113,114]

Published on 07 April 2020. Downloaded on 1/28/2026 4:44:51 PM.

$(C_3H_5N_2)_5[Bi_2Cl_{11}]$,[113] $(C_3H_5N_2)_5[Bi_2Br_{11}]$,[114] $(C_3H_5N_2)_5[Sb_2Br_{11}]$[123] (R = imidazolium) and $(C_5H_5NH_2)_5[Bi_2Br_{11}]$[115] (R = pyridinium) denoted as an aromatic subgroup.

Consequently, an analysis of phase symmetry indicates that the symmetry of the paraelectric phases of the aliphatic analogs is higher (orthorhombic symmetry) than that of the three remaining salts containing aromatic organic cations (monoclinic). The temperature range of the existence of ferroelectric phases in the aliphatic compounds stays within room temperature (except of the formamidinium analog), while in the aromatic compounds it is shifted by almost 150–180 K towards the low temperatures. Despite obvious structural differences between these two subgroups (aliphatic/aromatic), the following elements are common for the compounds of the $R_5M_2X_{11}$ type:

- PTs are continuous in nature;
- PTs are classified as an 'order–disorder' type;
- Close to T_c, a critical slowing down of the macroscopic relaxation time is observed;
- Molecular mechanism of the ferroelectric PT is dominated by the dynamics of the organic cations.

In the paraelectric phase, two out of five cations, being in a general position, are ordered, while the remaining three, (located at special positions) reveal an orientational disorder (two-site model, 180° reorientation). In the ferroelectric phase, all cations are ordered, however, the key input to P_s is given only by three out of five organic cations.

Another element that distinguishes the analyzed materials is the long-range dipole–dipole interaction. It determines both the values of P_s and the electric permittivity close to T_c. Methylammonium ferroelectrics mark themselves out by the higher values of P_s in the range of 2 – 3 μC cm^{-2} and ε_{max} 1 – 2 ×10^4, than those for the aromatic analogs. The value of P_s for the latter compounds is by almost one order, and for ε' almost by 1.5 order, lower than that for the former ones. This means that the long-range dipole–dipole interactions in the aliphatic ferroelectrics are much stronger than those in the aromatic ones. This in turn has an impact on the values of the PT temperatures. The stronger the dipole–dipole interaction the higher the values of T_c (Fig. 14).

The other property, which deserves to be compared, is the dynamic property of ferroelectrics, analyzed using the dielectric relaxation data. All $R_5M_2X_{11}$ ferroelectrics indicate the critical slowing down of the macroscopic relaxation time around T_c, a phenomenon typical only of the ferroelectrics with an 'order–disorder' mechanism of PT. What matters for these crystals is a difference in the values of the macroscopic dielectric relaxation time. The dielectric dispersion in a case of the aromatic analogs is limited to the kilohertz frequencies (10^2–10^4 Hz), while in the aliphatic ones it is shifted to the microwave range (10^{-8}–10^{-10} Hz). One of the reasons for such a difference may be the size of the inertia moments of the organic dipoles as well as the way, in which the cations are bound through the hydrogen bound networks. The imidazolium cations have much higher inertia moments than methylammonium and formamidinium.

The most mysterious phenomenon in the $R_5M_2X_{11}$ ferroelectric group is the molecular mechanism of PT. In this regard, two possible contributions must be taken into account:

(i) 'order–disorder'

(ii) 'displacive'

The first contribution (i) is related to the dynamics of the organic cations, *i.e.* orientational disorder. The typical feature of the ferroelectrics with a continuous PT is the critical slowing down of the macroscopic relaxation time and a significant entropy effect ($\Delta S > R \ln 2$) indicating the mechanism of type (i).

The other contribution, of the 'displacive' type (ii), is not proved by experimental methods; however, based on the structural data, there are reasons to believe that the distortion of the discrete bioctahedral units is likely to appear and, therefore, should be taken into account. This effect is well visible among the aliphatic ferroelectrics but it is marginal in aromatic ones. The distortion of the bioctahedra units causes a

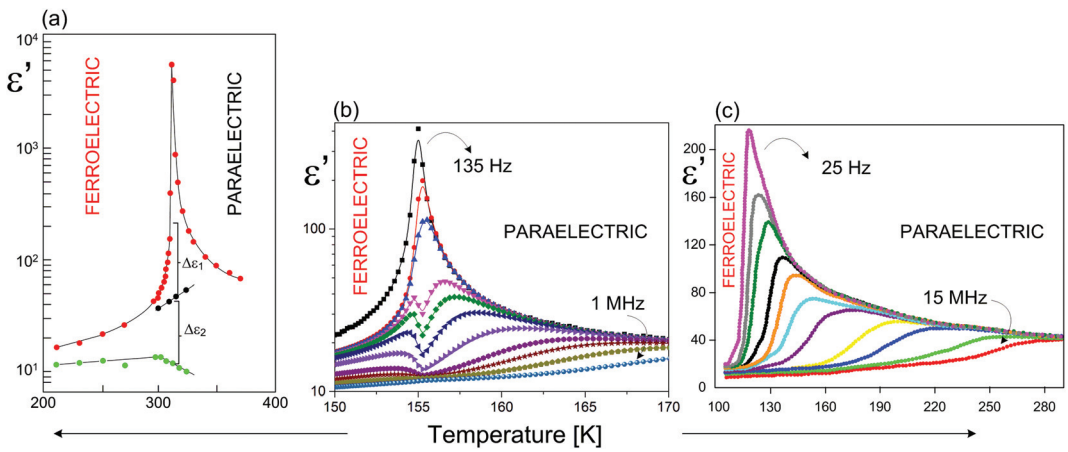

Fig. 14 Temperature dependence of the real part of the dielectric permittivity (ε') for (a) $(CH_3NH_3)_5[Bi_2Br_{11}]$[116–118] (MAPBB); (b) $(C_3H_5N_2)_5[Bi_2Br_{11}]$;[114] (c) $(C_5H_5NH)_5[Bi_2Br_{11}]$[115] around T_c.

 This journal is © the Partner Organisations 2020

Published on 07 April 2020. Downloaded on 1/28/2026 4:44:51 PM.

change in the negative charge distribution in the crystal structures, related to the halogen atoms; this subsequently leads to a change of the P_s values. There is one more factor necessary to analyze, namely, the electron lone pair effect. This effect should be attributed to the presence of the $6s^2$ electrons of Bi (III) atom, which is less polarizable than $5s^2$ electrons of Sb(III) atoms. All that leads to the conclusion that the anionic sublattice plays an important role in the generation of ferroelectricity in the $R_5M_2X_{11}$-type hybrids. Flexibility of the bioctahedral units (corner-sharing octahedra) may be a decisive parameter in the origin of spontaneous polarization.

3.5. R_3MX_6 type compounds and their modification (*e.g.* R′ R″$_2$ MX_6)

Recently a first halobismuthate(III) compound characterized by mixed organic networks has been reported by Wang *et al.*[161] The cationic substructure consists of two different molecules: one methylammonium (R′) and two benzylammonium (R″) ones as well as by an isolated octahedral unit $[BiBr_6]^{3-}$. $[(CH_3)_2NH_2][C_6H_5CH_2NH_2]_2BiBr_6$ appears to be a RT multiaxial ferroelectric with P_s = 1.0 μC cm^{-2}. The symmetry-breaking paraelectric–ferroelectric transformation is regarded in the Aizu notation as $\bar{3}mFm$ at 386 K. The molecular mechanism of the ferroelectric PT is assigned to the change in dynamics of the organic cations thus the transition is classified as an 'order–disorder' type. The discovery of a new type of connection of halobismuthates(III) with a mixed anionic substructure creates a new path to design molecular multiaxial ferroelectrics.

Although R_3MX_6-type compounds seem to be the 'poorest' with regard to their ferroelectricity, an interesting phenomenon, related to the imidazolium based hybrid, has been detected. The most spectacular result was the preparation of a new crystalline ferroelectric material ($(C_3H_5N_2)_5[Sb_2Br_{11}]$) using an *in situ* solid-state chemical reaction, where the starting substrate was $(C_3H_5N_2)_3[SbBr_6]\cdot H_2O$.[162]

4. Conclusions

In this review we present the attempts to find a correlation between crystal structures and polar/ferroelectric properties of haloantimonates(III) and halobismuthates(III). The materials under consideration are characterized by a rich diversity of the anionic sublattice (more than 40 types), nevertheless, the ferroelectric properties are limited only to four specific compositions: RMX_4, $R_3M_2X_9$, R_2MX_5, $R_5M_2X_{11}$. Of importance is that within the mentioned stoichiometry, the anionic network dimensions are also changed. One should note that so far already 31 ferroelectrics have been synthesized and fully characterized from the above mentioned family, which put them on one line with a well-known family of perovskite-type ferroelectric crystals (ABX_3, A_2BX_4).[164–167]

The RMX_4-type ferroelectrics (2 examples) indicate a 1D anionic structure, while the PTs are classified as a 'displacive' one. In the case of $R_3M_2X_9$ hybrids the ferroelectric ordering is observed only in the 0D (face-sharing bioctahedral species) and 2D inorganic lattice (corrugated layer structure and small organic cations). The molecular mechanism of the paraelectric–ferroelectric PTs for the 2D ferroelectrics is of the 'order–disorder' type. In turn for the 0D compounds the mechanism is quite complex because the 'order–disorder' and 'displacive' contributions are possible. Moreover, in the case of the $R_3M_2X_9$ complexes of the 2D-type the ferroelastic structure in both paraelectric and ferroelectric phases is observed (possible biferroics), however, the coupling between the corresponding order parameters, polarization and deformation, is very weak.

With regard to R_2MX_5 complexes, the ferroelectricity is conditioned by the presence of the 1D anionic structures with different modifications and the majority of PTs is of the 'displacive'-type with a minor 'order–disorder' contribution.

The $R_5M_2X_{11}$ hybrids are the most attractive from the viewpoint of polar properties. In this subclass, the inorganic part is created by the discrete anionic structures of the corner-sharing octahedra (0D-type). All of the $R_5M_2X_{11}$ crystals reveal ferroelectric properties. The molecular mechanism of the paraelectric–ferroelectric PT is not well recognized yet, however, the 'order–disorder' contribution, related to the dynamics of the organic cations, seems to play a key role. On the other hand the strong distortion of the anionic units as a result of the electron lone-pair effect ($5s^2$ (Sb) and $6s^2$ (Bi)) influences additionally the total polarization of the material. Of great importance is that aliphatic analogs, *e.g.* $(CH_3NH_3)_5[Bi_2Cl_{11}]$, $(CH_3NH_3)_5[Bi_2Br_{11}]$ and $(NH_2CHNH_2)_5[Sb_2Br_{11}]$ indicate dielectric properties similar to the well-known TGS (triglicyne sulphate) family and thus make them the most promising materials for applications.

It appears that not all stoichiometries have been analysed in terms of possible ferroelectric properties and R′R″$BiBr_6$ is the best example. It should be also added that the complexes of iodobismuthates(III), both with the organic cations (*e.g.* methylammonium) and with the monovalent metals (mixed cationic sublattice), are the most advantageous in the case of absorbing materials in solar cells. We anticipate that the broadening group of molecular–ionic ferroelectrics will help to develop rational structure–property relationships, leading to materials with precisely tunable characteristics.

Conflicts of interest

There are no conflicts to declare.

Acknowledgements

The paper is a result of the realization of the project no. UMO-2016/21/B/ST3/004640201/2078/17 financed by the National Science Centre, Poland (Prof. G. Bator).

References

1 G. Rijnders, S. Currás, M. Huijben, D. H. A. Blank and H. Rogalla, Influence of Substrate-Film Interface

Published on 07 April 2020. Downloaded on 1/28/2026 4:44:51 PM.

Engineering on the Superconducting Properties of $YBa_2Cu_3O_{7-\delta}$, *Appl. Phys. Lett.*, 2004, **84**, 1150.
2 J. F. Scott, Applications of Modern Ferroelectrics, *Science*, 2007, **315**, 954.
3 P. Hou, K. Yang, K. Ni, J. Wang, X. Zhong, M. Liao and S. Zheng, An Ultrathin Flexible Electronic Device Based on the Tunneling Effect: A Flexible Ferroelectric Tunnel Junction, *J. Mater. Chem. C*, 2018, **6**, 5193.
4 H. Gu, X. Qian, X. Li, B. Craven, W. Zhu, A. Cheng, S. C. Yao and Q. M. Zhang, Chip Scale Electrocaloric Effect Based Cooling Device, *Appl. Phys. Lett.*, 2013, **102**, 122904–122901.
5 Y. D. Wang, S. J. Smullin, M. J. Sheridan, Q. Wang, C. Eldershaw and D. E. Schwartz, A Heat-Switch-Based Electrocaloric Cooler, *Appl. Phys. Lett.*, 2015, **107**, 134103–134101.
6 J. F. Scott, F. D. Morrison, M. Miyake and P. Zubko, Nano-Ferroelectric Materials and Devices, *Ferroelectrics*, 2006, **336**, 237.
7 K. Gao, M. Gu, X. Qiu, X. N. Ying, H. Y. Ye, Y. Zhang, J. Sun, X. Meng, F. M. Zhang, D. Wu, H. L. Cai and X. S. Wu, Above-Room-Temperature Molecular Ferroelectric and Fast Switchable Dielectric of Diisopropylammonium Perchlorate, *J. Mater. Chem. C*, 2014, **2**, 9957.
8 M. Dawber, K. M. Rabe and J. F. Scott, Physics of Thin-Film Ferroelectric Oxides, *Rev. Mod. Phys.*, 2005, **77**, 1083.
9 G. Lupina, J. Dąbrowski, P. Dudek, G. Kozłowski, M. Lukosius, C. Wenger and H.-J. Müssig, Perovskite $BaHfO_3$ Dielectric Layers for Dynamic Random Access Memory Storage Capacitor Applications, *Adv. Eng. Mater.*, 2009, **11**, 259.
10 S. K. Kim, S. W. Lee, J. H. Han, B. Lee, S. Han and C. S. Hwang, Capacitors with an Equivalent Oxide Thickness of <0.5 nm for Nanoscale Electronic Semiconductor Memory, *Adv. Funct. Mater.*, 2010, **20**, 2989.
11 S. A. Adonin, M. N. Sokolov and V. P. Fedin, Bismuth(III) Halide Complexes: New Structural Types and New Application Areas, *Russ. J. Inorg. Chem.*, 2017, **62**, 1789.
12 B. Sun, L. Wei, H. Li and P. Chen, White-Light-Controlled Ferromagnetic and Ferroelectric Properties of Multiferroic Single-Crystalline $BiFeO_3$ Nanoflowers at Room Temperature, *J. Mater. Chem. C*, 2014, **2**, 7547.
13 D. Damjanovic, P. Muralt and N. Setter, Ferroelectric Sensors, *IEEE Sens. J.*, 2001, **1**, 191.
14 Y. Lee, J. Park, S. Cho, Y.-E. Shin, H. Lee, J. Kim, J. Myoung, S. Cho, S. Kang, C. Baig and H. Ko, Flexible Ferroelectric Sensors with Ultrahigh Pressure Sensitivity and Linear Response over Exceptionally Broad Pressure Range, *ACS Nano*, 2018, **12**, 4045.
15 X. Ren, Large electric-field-induced strain in ferroelectric crystals by point-defect-mediated reversible domain switching, *Nat. Mater.*, 2004, **3**, 91.
16 R. I. Epstein and K. J. Malloy, Electrocaloric Devices Based on Thin-Film Heat Switches, *J. Appl. Phys.*, 2009, **106**, 064509–064501.
17 K. Aizu, Possible Species of Ferromagnetic, Ferroelectric, and Ferroelastic Crystals, *Phys. Rev. B: Solid State*, 1970, **2**, 754.
18 J. Ma, U. Azhar, C. Zong, Y. Zhang, A. Xu, C. Zhai, L. Zhang and S. Zhang, Structured PVDF@BT Nanoparticles for Dielectric Materials: A Novel Composite to Prove the Dependence of Dielectric Properties on Ferroelectric Shell, *Mater. Des.*, 2019, **164**, 107556.
19 J. M. Gregg, Ferroelectrics at the Nanoscale, *Phys. Status Solidi A*, 2009, **206**, 577.
20 G. C. Xu, W. Zhang, X. M. Ma, Y. H. Chen, L. Zhang, H. L. Cai, Z. M. Wang, R. G. Xiong and S. Gao, Coexistence of Magnetic and Electric Orderings in the Metal-Formate Frameworks of $[NH_4][M(HCOO)_3]$, *J. Am. Chem. Soc.*, 2011, **133**, 14948.
21 R. Samantaray, R. J. Clark, E. S. Choi, H. Zhou and N. S. Dalal, $M_{3-x}(NH_4)_XCrO_8$ (M = Na, K, Rb, Cs): A New Family of Cr^{5+}-Based Magnetic Ferroelectrics, *J. Am. Chem. Soc.*, 2011, **133**, 3792.
22 A. Stroppa, P. Barone, P. Jain, J. M. Perez-Mato and S. Picozzi, Hybrid Improper Ferroelectricity in a Multiferroic and Magnetoelectric Metal-Organic Framework, *Adv. Mater.*, 2013, **25**, 2284.
23 Y. Y. Tang, W. Y. Zhang, P. F. Li, H. Y. Ye, Y. M. You and R. G. Xiong, Ultrafast Polarization Switching in a Biaxial Molecular Ferroelectric Thin Film: [Hdabco]ClO_4, *J. Am. Chem. Soc.*, 2016, **138**, 15784.
24 T. H. Moon, S. J. Oh and K. M. Ok, $[((R)\text{-}C_8H_{12}N)_4][Bi_2Br_{10}]$ and $[((S)\text{-}C_8H_{12}N)_4][Bi_2Br_{10}]$: Chiral Hybrid Bismuth Bromides Templated by Chiral Organic Cations, *ACS Omega*, 2018, **3**, 17895.
25 W. Zhang and R. G. Xiong, Ferroelectric Metal-Organic Frameworks, *Chem. Rev.*, 2012, **112**, 1163.
26 M. Ghasemi, M. Lyu, M. Roknuzzaman, J. H. Yun, M. Hao, D. He, Y. Bai, P. Chen, P. V. Bernhardt, K. Ostrikov and L. Wang, Phenethylammonium Bismuth Halides: From Single Crystals to Bulky-Organic Cation Promoted Thin-Film Deposition for Potential Optoelectronic Applications, *J. Mater. Chem. A*, 2019, **7**, 20733.
27 I. W. H. Oswald, E. M. Mozur, I. P. Moseley, H. Ahn and J. R. Neilson, Hybrid Charge-Transfer Semiconductors: $(C_7H_7)SbI_4$, $(C_7H_7)BiI_4$, and Their Halide Congeners, *Inorg. Chem.*, 2019, **58**, 5818.
28 B. Wagner, N. Dehnhardt, M. Schmid, B. P. Klein, L. Ruppenthal, P. Müller, M. Zugermeier, J. M. Gottfried, S. Lippert, M. U. Halbich, A. Rahimi-Iman and J. Heine, Color Change Effect in an Organic-Inorganic Hybrid Material Based on a Porphyrin Diacid, *J. Phys. Chem. C*, 2016, **120**, 28363.
29 R. Jakubas, G. Bator and Z. Ciunik, Halogenoantimonates (III) and halogenobismuthates(III)-a rich family of ferroelectric crystals, *Ferroelectrics*, 2003, **295**, 3.
30 S. A. Adonin, I. D. Gorokh, D. G. Samsonenko, I. V. Korol'kov, M. N. Sokolov and V. P. Fedin, Crystal Structures of Binuclear Bi(III) Chloride and Bromide

 This journal is © the Partner Organisations 2020

Published on 07 April 2020. Downloaded on 1/28/2026 4:44:51 PM.

Complexes with Some Cations—Alkylated Pyridine Derivatives, *J. Struct. Chem.*, 2017, **58**, 718.

31 S. A. Adonin, E. V. Peresypkina, M. N. Sokolov and V. P. Fedin, Iodobismuthate Complex $(Bu_4N)_3[Bi_3I_{12}]$: Crystal Structure of a New Polymorph, *J. Struct. Chem.*, 2015, **56**, 795.

32 S. A. Adonin, I. D. Gorokh, D. G. Samsonenko, A. S. Novikov, I. V. Korolkov, P. E. Plyusnin, M. N. Sokolov and V. P. Fedin, Binuclear and polymeric bromobismuthates complexes: Crystal structures and thermal stability, *Polyhedron*, 2019, **159**, 318.

33 S. A. Adonin, M. N. Sokolov and V. P. Fedin, Polyhalide-bonded metal complexes. Structural diversity in an electric class of compounds, *Coord. Chem. Rev.*, 2018, **367**, 1.

34 S. A. Adonin, M. N. Sokolov and V. P. Fedin, Polynuclear halide complexes of Bi(III): From structural diversity to the new properties, *Coord. Chem. Rev.*, 2016, **312**, 1.

35 S. A. Adonin, A. N. Usoltsev, A. S. Novikov, B. A. Kolesov, V. P. Fedin and M. N. Sokolov, One- and Two-Dimensional Iodine-Rich Iodobismuthates(III) Complexes: Structure, Optical Properties, and Features of Halogen Bonding in the Solid State, *Inorg. Chem.*, 2019, **58**, 15479.

36 A. M. Goforth, M. A. Tershansy, M. D. Smith, L. R. Peterson, J. G. Kelley, W. J. I. DeBenedetti and H.-C. Zur Loye, Structural Diversity and Thermochromic Properties of Iodobismuthate Materials Containing D-Metal Coordination Cations: Observation of a High Symmetry $[Bi_3I_{11}]^{2-}$ Anion and of Isolated I^- Anions, *J. Am. Chem. Soc.*, 2011, **133**, 603.

37 I. D. Gorokh, S. A. Adonin, P. A. Abramov, A. S. Novikov, M. N. Sokolov and V. P. Fedin, New strucutral type in polybromide-bromometalate hybrids: $(Me_3NH)_3\{[Bi_2Br_9](Br_2)\}$ - Crystal structure and theoretical studies of noncovalent Br···Br interactions, *Inorg. Chem. Commun.*, 2018, **98**, 169.

38 I. D. Gorokh, S. A. Adonin, D. G. Samsonenko, M. N. Sokolov and V. P. Fedin, Mono- and Binuclear Chloride and Bromide Complexes of Bi(III) with Double-Charged Cations Based on Pyridine: Synthesis and Crystal Structures, *Russ. J. Coord. Chem.*, 2018, **44**, 502.

39 M. L. Liu and L. H. Kong, Two novel trimethylaulfonium salts with polymeric $\{[SbCl_4]^-\}_n$ or $\{[CdCl_3]^-\}_n$ anions, *Acta Crystallogr.*, 2014, **C70**, 169.

40 N. Mercier, N. Louvain and W. Bi, Structural Diversity and Retro-Crystal Engineering Analysis of Iodometalate Hybrids, *CrystEngComm*, 2009, **11**, 720.

41 A. N. Usoltsev, M. Elshobaki, S. A. Adonin, L. A. Frolova, T. Derzhavskaya, P. A. Abramov, D. V. Anokhin, I. V. Korolkov, S. Y. Luchkin, N. N. Dremova, K. J. Stevenson, M. N. Sokolov, V. P. Fedin and P. A. Troshin, Polymeric Iodobismuthates $\{[Bi_3I_{10}]\}$ and $\{[BiI_4]\}$ with N-Heterocyclic Cations: Promising Perovskite-like Photoactive Materials for Electronic Devices, *J. Mater. Chem. A*, 2019, **7**, 5957.

42 S. A. Adonin, I. D. Gorokh, A. S. Novikov, P. A. Abramov, M. N. Sokolov and V. P. Fedin, Halogen Contacts-Induced Unusual Coloring in Bi^{III} Bromide Complex: Anion-to-Cation Charge Transfer via Br···Br Interactions, *Chem. – Eur. J.*, 2017, **23**, 15612.

43 S. A. Adonin, I. D. Gorokh, A. S. Novikov, D. G. Samsonenko, I. V. Korolkov, M. N. Sokolov and V. P. Fedin, Bromobismuthates: Cation-Induced Structural Diversity and Hirshfeld Surface Analysis of Cation–Anion Contacts, *Polyhedron*, 2018, **139**, 282.

44 S. A. Adonin, I. D. Gorokh, A. S. Novikov, D. G. Samsonenko, P. E. Plyusnin, M. N. Sokolov and V. P. Fedin, Bromine-Rich Complexes of Bismuth: Experimental and Theoretical Studies, *Dalton Trans.*, 2018, **47**, 2683.

45 S. K. Porter and R. A. Jacobson, Crystal Structure of Pyridinium Nonabromodiantimonate(III) Dibromide, *J. Chem. Soc.*, 1970, 1359.

46 B. Blažič and F. Lazarini, Structure of Diethylammonium Tetrachlorobismuthate(III), *Acta Crystallogr.*, 1985, **C41**, 1619.

47 A. Gągor, G. Banach, M. Węcławik, A. Piecha-Bisiorek and R. Jakubas, The Lone-Pair-Electron-Driven Phase Transition and Order-Disorder Processes in Thermochromic (2-MIm)SbI_4 Organic-Inorganic Hybrid, *Dalton Trans.*, 2017, **46**, 16605.

48 M. Owczarek, R. Jakubas, A. Pietraszko, W. Medycki and J. Baran, Investigation of Structure-Properties Relationship in a Novel Family of Halogenoantimonates (III) and Halogenobismuthates(III) with Morpholinium Cation: $[NH_2(C_2H_4)_2O]MX_4$]. Crystal Structure, Phase Transitions and Dynamics of Molecule, *Dalton Trans.*, 2013, **42**, 15069.

49 I. Płowaś, P. Szklarz, R. Jakubas and G. Bator, Structural, Thermal and Dielectric Studies on the Novel Solution Grown (4-Dimethylaminopyridinium) Chloroantimonate (III) and Chlorobismuthate(III) Crystals, *Mater. Res. Bull.*, 2011, **46**, 1177.

50 B. Kulicka, V. Kinzhybalo, R. Jakubas, Z. Ciunik, J. Baran and W. Medycki, Crystal Structure and Phase Transition of 4-Aminopyridinium Tetrachlorobismuthate(III), $[4\text{-}NH_2C_5H_4NH][BiCl_4]$, as Studied by x-Ray Diffraction, Dielectric, Proton NMR and Infrared Spectroscopy, *J. Phys.: Condens. Matter*, 2006, **18**, 5087.

51 R. Jakubas, Z. Ciunik and G. Bator, Ferroelectric Properties of $[4\text{-}NH_2C_5H_4NH][SbCl_4]$, *Phys. Rev. B: Condens. Matter Mater. Phys.*, 2003, **67**, 241031.

52 A. Gągor, Phase Transitions in Ferroelectric 4-Aminopyridinium Tetrachloroantimonate(III) – Revisited, *Acta Crystallogr.*, 2018, **B74**, 217.

53 M. Wojtaś, R. Jakubas, J. Zaleski, G. Bator and J. Baran, The Phase Situation and Ferroelectric Properties in the Mixed Crystals, *J. Mol. Struct.*, 2008, **887**, 262–268.

54 G. Xu, Y. Li, W. W. Zhou, G. J. Wang, X. F. Long, L. Z. Cai, M. S. Wang, G. C. Guo, J. S. Huang, G. Bator and R. Jakubas, A Ferroelectric Inorganic-Organic Hybrid Based on NLO-Phore Stilbazolium, *J. Mater. Chem.*, 2009, **19**, 2179.

55 A. Lipka, Preparation and Crystal structures of 2,2′ Bipyridinium Pentachloroantimonate $(C_{10}H_8N_2H_2)SbCl_5$

Published on 07 April 2020. Downloaded on 1/28/2026 4:44:51 PM.

and of the Metastable Modification of 4,4′ bypiridinium pentachloroantimonate $(C_{10}H_8N_2H_2)SbCl_5$, *Z. Naturforsch.*, 1983, **38b**, 1615.

56 U. Ensinger, W. Schwarz and A. Schmidt, Alkylammonium chloroantimonates(III). Structure and Vibrational Spectra, *Z. Naturforsch.*, 1983, **38b**, 149.

57 U. Ensinger, W. Schwarz and A. Schmidt, Tetraalkylammonium Tetrachloroantimonates(III). Structure and Vibrational spectra, *Z. Naturforsch.*, 1982, **37b**, 1584.

58 K. Kozawa and T. Uchida, Structures of Two Polymorphic Forms of Phenothiazine Tetrachloroantimonate, *Acta Crystallogr.*, 1990, **C46**, 1006.

59 A. L. Rheingold, A. D. Uhler and A. G. Landers, Synthesis, Crystal Structure, and Molecular Geometry of $[(\eta^5\text{-}C_5H_5)_2Fe]_4[Bi_4Br_{16}]$, the Ferrocenium Salt of a "Cluster of Octahedra" Hexadecabromotetrabismuthate Counterion, *Inorg. Chem.*, 1983, **22**, 3255.

60 L. Antolini, A. Benedetti, A. C. Fabretti and A. Giusti, Crystal and Molecular Structure, and Spectroscopic Characterization of Tetrakis(2-Amino-l,3,4-Thiadiazolium) Hexadecabromotetra-Antimonate(III), *J. Chem. Soc., Dalton Trans.*, 1988, 2501.

61 U. Geiser, E. Wade, H. H. Wang and J. M. Williams, Structure of a new iodobismuthate: tetra(n-butyl) ammonium 1,2;1,2;1,2;2,3;2,3;2,3-hexa-μ-iodo-1,1,1,3,3,3 hexaiodotribismuthate(III) (3:1), *Acta Crystallogr.*, 1990, **C46**, 1547.

62 B. Borgsen, F. Weller and K. Dehnicke, Uber Die Kronenetherkomplexe $[K(15\text{-Krone-}5)_2]_3[Sb_3I_{12}]$, $[TeCl_3(15\text{-Krone-}5)][TeCl_5]$ Und $[TeCl_3(15\text{-Krone-}5)]_2[TeCl_6]$, *Z. Anorg. Allg. Chem.*, 1991, **596**, 55.

63 S. G. Bott, L. Brammer, N. G. Connelly, M. Green, A. G. Orpen, J. F. Paxton, C. J. Schaverien, S. Bristow and N. C. Norman, Reactions of Co-ordinated Ligands, Part 48. Reactivity Studies of the Octatrienediyl-idenedimolybdenum Complexes $[Mo_2(\mu\text{-}C_8Me_8)(\eta\text{-}C_5H_5)_2]$ and $[Mo_2(\mu\text{-}C_8H_4But_4)(\eta\text{-}C_5H_5)_2]$. Crystal structures of $[Mo_2(\mu\text{-}C_8Me_7CH_2)\text{-}(\eta\text{-}C_5H_5)_2][CF_3SO_3]$, $[Mo_2(\mu\text{-}C_8Me_8)(\mu\text{-}Cl)_2(\eta\text{-}C_5H_5)_2][SbCl_4]\cdot CH_2Cl_2$ and $[Mo_2(\mu\text{-}C_8H_4But_4)(\mu_{MoC},\text{-}H)_2(\eta\text{-}C_5H_5)_2][BPh_4]\cdot CH_2Cl_2$, *J. Chem. Soc., Dalton Trans.*, 1990, **2**, 1957.

64 A. T. Mohammed and U. Muller, Tetraphenylphosphonium-Octabromodiantimonate, $(PPh_4)_2[Sb_2Br_8]$-Synthesis and Crystal Structure, *Z. Naturforsch.*, 1985, **40b**, 562.

65 S. Pohl, W. Saak, R. Lotz and D. Haase, On the Existence of Weak Interactions between Sb(III) and Phenyl Groups: $Sb_2Br_6(SPPh_3)_2$, $Sb_2I_6(SePPh_3)_2\cdot 2CH_2Cl_2$, $Sb_4Br_{12}(SPMe_2Ph)_4$ and $(Ph_4P)_2Sb_2Br_8\cdot CH_3CN$, *Z. Naturforsch.*, 1990, **45b**, 1355.

66 N. W. Alcock, M. Ravindran and G. R. Willey, Crown Ether Complexes of Bi^{III}. Synthesis and Crystal and Molecular Structures of $BiCl_3\cdot$12-Crown-4 and $2BiCl_3\cdot$18-Crown-6, *J. Chem. Soc., Chem. Commun.*, 1989, **52**, 1063.

67 M. Wojciechowska, P. Szklarz, A. Białońska, J. Baran, R. Janicki, W. Medycki, P. Durlak, A. Piecha-Bisiorek and R. Jakubas, Enormous Lattice Distortion through an Isomorphous Phase Transition in an Organic-Inorganic Hybrid Based on Haloantimonate(III), *CrystEngComm*, 2016, **18**, 6184.

68 A. Piecha-Bisiorek, K. Mencel, V. Kinzhybalo, A. Szota, R. Jakubas, W. Medycki and W. Zawrocki, Ferroelasticity and Piezoelectricity of Organic-Inorganic Hybrid Materials with a One-Dimensional Anionic Structure: So Similar, yet so Different, *CrystEngComm*, 2018, **20**, 2112.

69 J. Belz, R. Wber, A. Roloff and B. Ross, Crystal structure of bis(Tert.-Butylammonium)- Di-μ -Chloro-Trichloroantimonate, $(C_4H_{12}N)_2Sb_2Cl_8$, *Z. Kristallogr. – Cryst. Mater.*, 1992, **202**, 281.

70 H.-J. Lubberger, E. Muller, J. Hofmann, H. Fischer and J. C. Jochims, Reactions of 1-Thia-3-azoniabutatriene Salts with Alcohols, Carbonyl Compounds, Diazoalkanes, Nitrile Oxides, Nitrones, Enamines, and Butadienes, *Chem. Ber.*, 1991, **124**, 2537.

71 K. Kihara and T. Sudo, The Crystal Structures of β-$Cs_3Sb_2Cl_9$ and $Cs_3Bi_2Cl_9$, *Acta Crystallogr.*, 1974, **B30**, 1088.

72 R. Jakubas, Z. Czapla, Z. Galewski, L. Sobczyk, O. J. Żogał and T. Lis, Structure and Phase Transition in $(CH_3NH_2)_3Sb_2Cl_9$, *Phys. Status Solidi*, 1986, **93**, 449.

73 R. Jakubas, G. Bator, J. Zaleski, A. Pietraszko and R. Decressain, The Structure and Phase Transition of $(CH_3NH_3)_3Sb_{2(1-X)}Bi_{2x}Cl_9$ Mixed Crystals, *J. Phys.: Condens. Matter*, 1996, **8**, 367.

74 H. Ishihara, K. Yamada, T. Okuda and A. Weisz, The Structures of $M_2X_9^{3-}$ (M = Bi: X = Cl, Br) Ions Determined by Rietveld Analysis of X-Ray Powder Diffraction Data, *Bull. Chem. Soc. Jpn.*, 1993, **66**, 380.

75 P. Ciąpała, J. Zaleski, G. Bator, R. Jakubas and A. Pietraszko, The Structure and Phase Transition of Tris (n−Propylammonium) Enneachlorodiantimonate(III), $(n\text{-}C_3H_7NH_3)_3Sb_2Cl_9$, *J. Phys.: Condens. Matter*, 1996, **8**, 1957.

76 V. G. Meyer and A. Schonemund, Zur Kenntnis der Hochtemperatur-Phasenumwandlung bei $Cs_3Bi_2Cl_9$, *Z. Anorg. Allg. Chem.*, 1980, **468**, 185.

77 A. Piecha, V. Kinzhybalo, K. Ślepokura and R. Jakubas, Characterization, Thermal and Electric Properties of Imidazolium Bromoantimonate(III): $[C_3H_5N_2]_3[Sb_2Br_9]$, *J. Solid State Chem.*, 2007, **180**, 265.

78 M. Bujak and J. Zaleski, High temperature ferro-paraelectric phase transition in tris(trimethylammonium) nonachlorodiantimonate(III) (TMACA) studied by X-ray diffraction method, *Cryst. Eng.*, 2001, **4**, 241.

79 R. Jakubas, E. Narewski and L. Sobczyk, High Frequency Dielectric Dispersion in $[(CH_3)_3NH]_3Sb_2Cl_9$, *Phys. Status Solidi*, 1986, **98**, K115.

80 M. Wojciechowska, A. Gągor, A. Piecha-Bisiorek, R. Jakubas, A. Cizman, J. K. Zaręba, M. Nyk, P. Zieliński, W. Medycki and A. Bil, Ferroelectricity and Ferroelasticity in Organic Inorganic Hybrid $(Pyrrolidinium)_3[Sb_2Cl_9]$, *Chem. Mater.*, 2018, **30**, 4597.

 This journal is © the Partner Organisations 2020

Published on 07 April 2020. Downloaded on 1/28/2026 4:44:51 PM.

81 J. Mróz and R. Jakubas, Ferroelectric and Ferroelastic Phase Transitions in $(CH_3NH_3)_3Sb_2Br_9$ Crystals, *Ferroelectr. Lett. Sect.*, 1994, **17**, 73.
82 R. Jakubas, G. Bator, L. Sobczyk and J. Mróz, Ferroelectrics Dielectric and Pyroelectric Properties Crystals in the Ferroelectric Phase Transition Regions, *Ferroelectrics*, 1994, **158**, 43.
83 G. Bator, R. Jakubas, L. Sobczyk and J. Mróz, Dielectric and Pyroelectric Properties of $[N(CH_3)_3H]_3Sb_2Cl_9$ in the Low Temperature Region, *Ferroelectrics*, 1993, **141**, 177.
84 R. Jakubas and L. Sobczyk, Phase Transitions in Alkylammonium Halogenoantimonates and Bismuthates, *Phase Transitions*, 1990, **20**, 163.
85 R. Jakubas, U. Krzewska, G. Bator and L. Sobczyk, Structure and Phase Transition in $(CH_3NH_3)_3Bi_2Br_9$. A Novel Improper Ferroelectrics, *Ferroelectrics*, 1988, **77**, 129.
86 J. Zaleski, C. Pawlaczyk, R. Jakubas and H.-G. Unruh, Related Content Structure and Dynamic Dielectric Behaviour of Review, *J. Phys.: Condens. Matter*, 2000, **12**, 7509.
87 A. Miniewicz and R. Jakubas, Pyroelectric Properties and Phase Transition in Tris(Dimethylammonium)nonabromodiantimonate(III), *Solid State Commun.*, 1988, **67**, 1079.
88 J. Zaleski and A. Pietraszko, Structure at 200 and 298 K and X-Ray Investigations of the Phase Transition at 242 K of $[NH_2(CH_3)_2]_3Sb_2Cl_9$ (DMACA), *Acta Crystallogr.*, 1996, **B52**, 287.
89 A. Kallel and J. W. Bats, Tris(Trimethylammonium) Nonachlorodiantimonate(III), $[NH(CH_3)_3]_3[Sb_2Cl_9]$, *Acta Crystallogr.*, 1985, **C41**, 1022.
90 F. Lazarini, Tetraphenylphosphonium Enneabromodibismuthate(III), *Acta Crystallogr.*, 1977, **33**, 2686.
91 C. R. Hubbard and R. A. Jacobson, Molecular Bromine Bridging of $Sb^{III}{}_2Br_9{}^{3-}$ Anions and the Crystal Structure of Tetramethylammonium Nonabromodiantimonate(III)-Dibromine, *Inorg. Chem.*, 1972, **11**, 2247.
92 M. Hall, M. Nunn, M. J. Begley and D. B. Sowerby, Nonahalogenodiantimon(III)ates; their preparation and the crystal structures of $[Hpy]_3[Sb_2Cl_9]$, $[nMe_4]_3[Sb_2Br_9]$, and $[nMe_4]_3[Sb_2Br_3Cl_6]$, *J. Chem. Soc., Dalton Trans.*, 1986, 1231.
93 M. Węcławik, A. Gągor, R. Jakubas, A. Piecha-Bisiorek, W. Medycki, J. Baran, P. Zieliński and M. Gałązka, Structure-Property Relationships in Hybrid $(C_3H_5N_2)_3[Sb_2I_9]$ and $(C_3H_5N_2)_3[Bi_2I_9]$ Isomorphs, *Inorg. Chem. Front.*, 2016, **3**, 1306.
94 P. Szklarz, R. Jakubas, A. Piecha-Bisiorek, G. Bator, M. Chański, W. Medycki and J. Wuttke, Organic-Inorganic Hybrid Crystals, $(2,4,6\text{-}CH_3PyH)_3Sb_2Cl_9$ and $(2,4,6\text{-}CH_3PyH)_3Bi_2Cl_9$. Crystal Structure Characterization and Tunneling of CH_3 Groups Studied by ^1H NMR and Neutron Spectroscopy, *Polyhedron*, 2018, **139**, 249.
95 B. Aurivillius and C. Stalhandske, The Crystal Structure of a Tetranuclear Bismuth(III) Complexes, $(C_5H_5NH)_6Bi_4Cl_{18}$, *Acta Chem. Scand., Ser. A*, 1978, **32**, 715.
96 A. Piecha, R. Jakubas, V. Kinzhybalo and W. Medycki, Crystal Structure, Dielectric Properties and Molecular Motions of Molecules in Thiazolium Halometalates(III): $(C_3H_4NS)_6M_4Br_{18}\cdot 2H_2O$ (M = Sb, Bi), *J. Mol. Struct.*, 2012, **1013**, 55.
97 A. Piecha, R. Jakubas, V. Kinzhybalo and T. Lis, Structural and Dielectric Properties of Thiazolium Chlorobismuthate (III) and Chloroantimonate(III), *J. Mol. Struct.*, 2008, **887**, 194.
98 A. Piecha, R. Jakubas, A. Pietraszko, J. Baran, W. Medycki and D. Kruk, Structural Characterization, Thermal, Dielectric, Vibrational Properties and Molecular Motions in $[C_3N_2H_5]_6[Bi_4Br_{18}]$, *J. Solid State Chem.*, 2009, **182**, 2949.
99 A. Piecha, R. Jakubas and A. Pietraszko, Phase Transitions and Electric Properties of Imidazolium Chlorobismuthate (III): $[C_3H_5N_2]_6[Bi_4Cl_{18}]$, *J. Mol. Struct.*, 2007, **829**, 149.
100 M. Ksiądzyna, A. Gągor, A. Piecha-Bisiorek, A. Ciżman, W. Medycki and R. Jakubas, Exploring a Hybrid Ferroelectric with a 1-D Perovskite-like Structure: Bis (Pyrrolidinium) Pentachloroantimonate(III), *J. Mater. Chem. C*, 2019, **7**, 10360.
101 Z. Yin, J. X. Gao, H. P. Chen and W. Q. Liao, An Above-Room-Temperature Phase Transition with Dielectric-Switching Properties in a Halogenobismuthate(III) – Tris (Cyclohexylmethylammonium) Pentabromobismuthate (III) Bromide, *Eur. J. Inorg. Chem.*, 2017, **2017**, 3555.
102 A. Piecha-Bisiorek, A. Gągor, R. Jakubas, A. Ciżman, R. Janicki and W. Medycki, Ferroelectricity in Bis (Ethylammonium) Pentachlorobismuthate(III): Synthesis, Structure, Polar and Spectroscopic Properties, *Inorg. Chem. Front.*, 2017, **4**, 1281.
103 C. Y. Mao, W. Q. Liao, Z. X. Wang, Z. Zafar, P. F. Li, X. H. Lv and D. W. Fu, Temperature-Triggered Dielectric-Optical Duple Switch Based on an Organic-Inorganic Hybrid Phase Transition Crystal: $[C_5N_2H_{16}]_2SbBr_5$, *Inorg. Chem.*, 2016, **55**, 7661.
104 C. Y. Mao, W. Q. Liao, Z. X. Wang, P. F. Li, X. H. Lv, H. Y. Ye and Y. Zhang, Structural Characterization, Phase Transition and Switchable Dielectric Behaviors in a New Zigzag Chain Organic-Inorganic Hybrid Compound: $[C_3H_7NH_3]_2SbI_5$, *Dalton Trans.*, 2016, **45**, 5229.
105 T. B. Rhaiem, H. Boughzala and A. Van Der Lee, Crystal Structure of a New Hybrid Antimony-Halide-Based Compound for Possible Non-Linear Optical Applications, *Acta Crystallogr.*, 2015, **E71**, 498.
106 N. Mercier, The Templating Effect and Photochemistry of Viologens in Halometalate Hybrid Crystals, *Eur. J. Inorg. Chem.*, 2013, 19.
107 N. Leblanc, N. Mercier, L. Zorina, S. Simonov, P. Auban-Senzier and C. Pasquier, Spontaneous Polarization and Clear Hysteresis Loop of a Room-Temperature Hybrid Ferroelectric Based on Mixed-Halide $[BiI_3Cl_2]$ Polar Chains and Methylviologen Dication, *J. Am. Chem. Soc.*, 2011, **133**, 14924.
108 M. Owczarek, P. Szklarz, R. Jakubas and A. Miniewicz, MX_5: A New Family of Morpholinium Nonlinear Optical Materials among Halogenoantimonate(III) and

Published on 07 April 2020. Downloaded on 1/28/2026 4:44:51 PM.

Halogenobismuthate(III) Compounds. Structural Characterization, Dielectric and Piezoelectric Properties, *Dalton Trans.*, 2012, **41**, 7285.

109 M. Moskwa, G. Bator, M. Rok, W. Medycki, A. Miniewicz and R. Jakubas, Investigations of Organic-Inorganic Hybrids Based on Homopiperidinium Cation with Haloantimonates(III) and Halobismuthates(III). Crystal Structures, Reversible Phase Transitions, Semiconducting and Molecular Dynamic Properties, *Dalton Trans.*, 2018, **47**, 13507.

110 F. Bigoli, M. Lanfranchi and M. A. Pellinghelli, The structures of bis($1H^+$,$5H^+$-S-methylisothiocarbonohydrazidium) di-μ-chloro-octachlorodibismuthate(III) tetrahydrate and tris($1H^+$-S-methylisothiocarbonohydrazidium) esachlorobismuthate(III), *Inorg. Chim. Acta*, 1984, **90**, 215.

111 A. Piecha, V. Kinzhybalo, R. Jakubas, J. Baran and W. Medycki, Structural Characterization, Molecular Dynamics, Dielectric and Spectroscopic Properties of Tetrakis(Pyrazolium) Bis(M2-Bromo-Tetrabromobismuthate(III)) Dihydrate, $[C_3N_2H_5]_4[Bi_2Br_{10}]\cdot 2H_2O$, *Solid State Sci.*, 2007, **9**, 1036.

112 M. Moskwa, G. Bator, A. Piecha-Bisiorek, R. Jakubas, W. Medycki, A. Ciżman and J. Baran, X-Ray Structure and Investigation of Molecular Motions by Dielectric, Vibrational and ^1H NMR Methods for Two Organic-Inorganic Hybrid Piperazinium Compounds: $(C_4H_{12}N_2)_2[Sb_2Cl_{10}]\cdot 2H_2O$ and $(C_4H_{12}N_2)_2[Sb_2Br_{10}]\cdot 2H_2O$, *Mater. Res. Bull.*, 2018, **104**, 202.

113 R. Jakubas, A. Piecha, A. Pietraszko and G. Bator, Structure and Ferroelectric Properties of $(C_3N_2H_5)_5Bi_2Cl_{11}$, *Phys. Rev. B: Condens. Matter Mater. Phys.*, 2005, **72**, 1.

114 A. Piecha, A. Białońska and R. Jakubas, Structure and Ferroelectric Properties of $[C_3N_2H_5]_5[Bi_2Br_{11}]$, *J. Phys.: Condens. Matter*, 2008, **20**, 325224.

115 J. Jóźków, R. Jakubas, G. Bator and A. Pietraszko, Ferroelectric Properties of $(C_5H_5NH)_5Bi_2Br_{11}$, *J. Chem. Phys.*, 2001, **114**, 7239.

116 C. Pawlaczyk, H. Motsch, R. Jakubas and H.-G. Unruh, Dielectric behaviour of the new ferroelectric $(CH_3NH_3)_5Bi_2Br_{11}$ in the microwave region, *Ferroelectrics*, 1990, **108**, 127.

117 C. Pawlaczyk, R. Jakubas, K. Planta, C. Bruch, J. Stephan and H.-G. Unruh, Dynamic Dielectric Behaviour of $(CH_3NH_3)_5Bi_2X_{11}$ (X: Br, CI) Single Crystals, *Ferroelectrics*, 1992, **126**, 145.

118 M. Połomska and R. Jakubas, Dynamics of Ferroelectric Domains in $(CH_3NH_3)_5Bi_2Br_{11}$ Studied by Liquid Crystal Decoration Technique, *Ferroelectrics*, 1990, **106**, 57.

119 J. Lefebvre, P. Carpentier and R. Jakubas, Structures and Phase Transition in the Ferroelectric Crystal of Pentakis (Methylammonium) Undecachlorodibismuthate(III): $[NH_3(CH_3)]_5Bi_2Cl_{11}$, *Acta Crystallogr.*, 1991, **B47**, 228.

120 P. Carpentier, J. Lefebvre and R. Jakubas, Structure of Pentakis(Methylammonium) Undecachlorodibismuthate (III), $[NH_3(CH_3)]_5Bi_2Cl_{11}$, at 130 K and Mechanism of the Phase Transitions, *Acta Crystallogr.*, 1995, **B51**, 167.

121 R. Jakubas, A New Ferroelectric Compound: $(CH_3NH_3)_5Bi_2Br_{11}$, *Solid State Commun.*, 1989, **69**, 267.

122 R. Cach and R. Jakubas, Determination of Landau-energy parameters by dielectric measurements in $(CH_3NH_3)_5Bi_2Cl_{11}$ crystals, *Ferroelectrics*, 1990, **108**, 121.

123 A. Piecha, A. Pietraszko, G. Bator and R. Jakubas, Structural Characterization and Ferroelectric Ordering in $(C_3N_2H_5)_5Sb_2Br_{11}$, *J. Solid State Chem.*, 2008, **181**, 1155.

124 F. Lazarini, Structure of Diethylammonium Hexa-bromobismuthate (III), *Acta Crystallogr.*, 1985, **C41**, 1617.

125 W. G. McPherson and E. A. Meyers, The Crystal Structures of Bismuth Halide Complex Salts. III. Tris (Dimethylammonium) Hexabromobismuthate(III), $[(CH_3)_2NH_2]_3BiBr_6$, *J. Phys. Chem.*, 1968, **72**, 3117.

126 L. R. Morrs and W. R. Robinson, Crystal Structure of $Cs_2NaBiCl_6$, *Acta Crystallogr.*, 1972, **B28**, 653.

127 F. Lazarini, Structure of Diethylammonium Hexachlorobismuthate(III), *Acta Crystallogr.*, 1987, **C43**, 637.

128 S. Jarraya, A. B. Salah, A. Daoud, W. Rothammel and H. Burzlaff, Structure of $[(C_2H_5)_2NH_2]_3BiCl_6$, *Acta Crystallogr.*, 1993, **C49**, 1594.

129 M. Bujak, Formation and Distortion of Iodidoantimonates (III): The First Isolated $[SbI_6]^{3-}$ Octahedron, *Acta Crystallogr.*, 2017, **B73**, 432.

130 A. Piecha, A. Gągor, M. Węcławik, R. Jakubas and W. Medycki, Anomalous Dielectric Behaviour in Centrosymmetric Organic-Inorganic Hybrid Chlorobismuthate(III) Containing Functional N, N-Dimethylethylammonium Ligand. Crystal Structure and Properties, *Mater. Res. Bull.*, 2013, **48**, 151.

131 M. Chański, A. Białońska, R. Jakubas and A. Piecha-Bisiorek, Structural Characterization and Properties of Bis (1,4-H_2-1,2,4-Triazolium) Pentachlorobismuthate (III) and Cocrystal of Ammonium Chloride with Tris (1,4-H_2-1,2,4-Triazolium) Hexachlorobismuthate (III), *Polyhedron*, 2014, **71**, 69.

132 I. Płowaś, G. Bator, R. Jakubas and J. Baran, Thermal, Dielectric and Vibrational Properties of Allylammonium Chloroantimonates(III) and Chlorobismuthates(III): $[C_3H_5NH_3]_3[BiCl_6]$ and $[C_3H_5NH_3]_3[SbCl_5]Cl$, *Vib. Spectrosc.*, 2012, **62**, 121.

133 I. Płowaś, A. Białońska, G. Bator, R. Jakubas, W. Medycki and J. Baran, Tris(Allylammonium) Hexabromobismuthate(III) - Crystal Structure, Phase Transitions and Thermal, Dielectric, Vibrational and ^1H NMR Properties over a Range of Temperatures, *Eur. J. Inorg. Chem.*, 2012, 636.

134 J. Tarasiewicz, R. Jakubas, G. Bator, J. Zaleski, J. Baran and W. Medycki, Structural Characterization, Thermal, Dielectric, Vibrational Properties and Molecular Dynamics of $(C_5H_5NH)_3BiCl_6$, *J. Mol. Struct.*, 2009, **932**, 6.

135 B. Kulicka, R. Jakubas, B. Bednarska-Bolek, G. Bator and Z. Ciunik, Crystal Structure and Phase Transitions in Dipropylammonium Hexachloroantimonate(v): $[N(C_3H_7)_2H_2][SbCl_6]$, *J. Mol. Struct.*, 2006, **792–793**, 151.

 This journal is © the Partner Organisations 2020

Published on 07 April 2020. Downloaded on 1/28/2026 4:44:51 PM.

136 L. Sobczyk, R. Jakubas and J. Zaleski, Self-Assembly of Sb(III) and Bi(III) Halo-Coordinated Octahedra in Salts of Organic Cations. Structure, Properties and Phase Transitions, *Pol. J. Chem.*, 1997, **71**, 265.

137 R. D. Rogers, A. H. Bond and S. Aguinaga, Alcoholysis of $Bi(NO_3)_3{\cdot}5H_2O$ by Polyethylene Glycols. Comparison with Bismuth(III) Nitrate Crown Ether Complexation, *J. Am. Chem. Soc.*, 1992, **114**, 2960.

138 S. Pohl, R. Lötz, D. Haase and W. Saak, Iodoantimonates of compositions $A^+Sb_2I_7^-$: Discrete Anions in $(Me_4N)_4Sb_8I_{28}$ and $(Me_3S)_4Sb_8I_{28}$, polymeric chains in $(Me_3NCH_2Ph)Sb_2I_7$ (Me = CH_3, Ph = C_6H_5), *Z. Naturforsch.*, 1988, **43b**, 1144.

139 S. Pohl, W. Saak and D. Haase, Synthesis and crystal structure of $(Ph_4P)_4Sb_8I_{28}$ and $(Ph_4P)Sb_3I_{10}$ (Ph = C_6H_5), *Z. Naturforsch.*, 1987, **42b**, 1493.

140 B. S. Pohl, W. Saak, P. Mayer and A. Schmidpeter, $[Sb_3I_{10}^-]_\infty$ A Polymeric Anion with Transitions from Trigonal Pyramidal to Octahedral Coordination of Antimony(III), *Angew. Chem., Int. Ed. Engl.*, 1986, **25**, 825.

141 C. J. Carmalt, N. C. Norman and L. J. Farrugia, The Structure of an Unusual Polymeric Iodoantimonate(III) Anion with Disordered Antimony Sites, *Polyhedron*, 1994, **13**, 1655.

142 S. Pohl, M. Peters, D. Haase and W. Saak, Formation of Iodoantimonates and Bismuthates. Crystal Structures of $(PhCH_2NEt_3)_4[Sb_6I_{22}]$, $(PhCH_2NEt_3)_4[Bi_6I_{22}]$ and $(Ph_4P)_3[Bi_5I_{18}]$, *Z. Naturforsch.*, 1994, **49b**, 741.

143 S. Pohl, R. Lotz, W. Saak and D. Haase, Structural Diversity in Iodoantimonates; the Anions $Sb_3I_{11}^{2-}$, $Sb_5I_{18}^{3-}$ and $Sb_6I_{22}^{4-}$, *Angew. Chem., Int. Ed. Engl.*, 1989, **28**, 344.

144 S. Pohl, D. Haase, R. Lötz and W. Saak, $[Fe(phen)_3]_2Sb_6I_{22}{\cdot}2CH_3CN$: An Iodoantimonate with Central $[Sb_6I_6]$-Double Cube (phen = 1,10-Phenanthrolin), *Z. Naturforsch.*, 1988, **43b**, 1033.

145 T. Zaleski, T. Głowiak, R. Jakubas and L. Sobczyk, Crystal structure and phase transitions of $[(C_2H_5)_4N]_6Bi_8Cl_{30}$, *J. Phys. Chem. Solids*, 1989, **50**, 1265.

146 G. Bator and R. Jakubas, Dynamical Dielectric Properties of $[4\text{-}NH_2C_5H_4NH][SbCl_4]$ in the Incommensurate Phase, *J. Phys. Soc. Jpn.*, 2003, **72**, 2369.

147 R. Jakubas, J. Zaleski and L. Sobczyk, Phase Transitions in $(CH_3NH_3)_3Bi_2I_9$ (MAIB), *Ferroelectrics*, 1990, **108**, 109.

148 M. E. Kamminga, A. Stroppa, S. Picozzi, M. Chislov, I. A. Zvereva, J. Baas, A. Meetsma, G. R. Blake and T. T. M. Palstra, Polar Nature of $(CH_3NH_3)_3Bi_2I_9$ Perovskite-Like Hybrids, *Inorg. Chem.*, 2017, **56**, 33.

149 C. Ji, Z. Sun, A. Zeb, S. Liu, J. Zhang, M. Hong and J. Luo, Bandgap Narrowing of Lead-Free Perovskite-Type Hybrids for Visible-Light-Absorbing Ferroelectric Semiconductors, *J. Phys. Chem. Lett.*, 2017, **8**, 2012.

150 Z. Sun, A. Zeb, S. Liu, C. Ji, T. Khan, L. Li, M. Hong and J. Luo, Exploring a Lead-Free Semiconducting Hybrid Ferroelectric with a Zero-Dimensional Perovskite-like Structure, *Angew. Chem., Int. Ed.*, 2016, **55**, 11854.

151 P. Szklarz, A. Gągor, R. Jakubas, P. Zieliński, A. Piecha-Bisiorek, J. Cichos, M. Karbowiak, G. Bator and A. Cizman, Lead-Free Hybrid Ferroelectric Material Based on Formamidine: $[NH_2CHNH_2]_3Bi_2I_9$, *J. Mater. Chem. C*, 2019, **7**, 3003.

152 P. Szklarz, R. Jakubas, A. Gągor, G. Bator, J. Cichos and M. Karbowiak, $[NH_2CHNH_2]_3Sb_2I_9$: A Lead-Free and Low-Toxicity Organic–Inorganic Hybrid Ferroelectric Based on Antimony(III) as a Potential Semiconducting Absorber, *Inorg. Chem. Front.*, 2020, **7**, 1780.

153 J. Zhang, S. Han, C. Ji, W. Zhang, Y. Wang and K. Tao, $[(CH_3)_3NH]_3Bi_2I_9$: A Polar Lead-Free Hybrid Perovskite-Like Material as a Potential Semiconducting Absorber, *Chem. – Eur. J.*, 2017, **23**, 17304.

154 H. Y. Zhang, Z. Wei, P. F. Li, Y. Y. Tang, W. Q. Liao, H. Y. Ye, H. Cai and R. G. Xiong, The Narrowest Band Gap Ever Observed in Molecular Ferroelectrics: Hexane-1,6-Diammonium Pentaiodobismuth(III), *Angew. Chem., Int. Ed.*, 2018, **57**, 526–530.

155 Y. Wang, C. Shi and X.-B. Han, Organic–Inorganic Hybrid $[H_2mdap][BiCl_5]$ Showing an above-Room-Temperature Ferroelectric Transition with Combined Order–Disorder and Displacive Origins, *Polyhedron*, 2017, **133**, 132.

156 P. Li, Y. Tang, W. Liao, H. Ye, Y. Zhang, D. Fu and Y. You, Semiconducting Molecular Ferroelectric with a Bandgap Much Lower than That of $BiFeO_3$, *NPG Asia Mater.*, 2017, **9**, 1.

157 W. Bi, N. Leblanc, N. Mercier, P. Auban-Senzier and C. Pasquier, Thermally Induced Bi(III) Lone Pair Stereoactivity: Ferroelectric Phase Transition and Semiconducting Properties of $(MV)BiBr_5$ (MV = Methylviologen), *Chem. Mater.*, 2009, **21**, 4099.

158 A. Piecha, A. Białońska and R. Jakubas, Novel Organic-Inorganic Hybrid Ferroelectric: Bis(Imidazolium) Pentachloroantimonate(III), $(C_3N_2H_5)_2SbCl_5$, *J. Mater. Chem.*, 2012, **22**, 333.

159 R. Jakubas, A. Gągor, M. J. Winiarski, M. Ptak, A. Piecha-Bisiorek and A. Ciżman, Ferroelectricity in Ethylammonium Bismuth-Based Organic-Inorganic Hybrid: $(C_2H_5NH_3)_2[BiBr_5]$, *Inorg. Chem.*, 2020, **59**, 3417.

160 W. P. Zhao, C. Shi, A. Stroppa, D. Di Sante, F. Cimpoesu and W. Zhang, Lone-Pair-Electron-Driven Ionic Displacements in a Ferroelectric Metal-Organic Hybrid, *Inorg. Chem.*, 2016, **55**, 10337.

161 B. Wang, D. Ma, H. Zhao, L. Long and L. Zheng, Room Temperature Lead-Free Multiaxial Inorganic-Organic Hybrid Ferroelectric, *Inorg. Chem.*, 2019, **58**, 13953–13959.

162 A. Piecha, A. Gągor, A. Pietraszko and R. Jakubas, Unprecedented Solid-State Chemical Reaction - From $(C_3N_2H_5)_3SbBr_6{\cdot}H_2O$ to $(C_3N_2H_5)_5Sb_2Br_{11}$. From Centrosymmetric to Non-Centrosymmetric Crystal Structure, *J. Solid State Chem.*, 2010, **183**, 3058.

163 K. Mencel, A. Gągor, R. Jakubas, A. Ciżman, W. Medycki, J. K. Zaręba and A. Piecha-Bisiorek, Ferroelectricity in Lead Free Organic-Inorganic 0D Hybrid: Formamidinium Bromoantimonate(III), *J. Mater. Chem. C*, DOI: 10.1039/d0tc00168f.

164 H. Y. Ye, Y. Y. Tang, P. F. Li, W. Q. Liao, J. X. Gao, X. N. Hua, H. Cai, P. P. Shi, Y. M. You and R. G. Xiong, Metal-Free Three-Dimensional Perovskite Ferroelectrics, *Science*, 2018, **361**, 151–155.
165 Y. M. You, W. Q. Liao, D. Zhao, H. Y. Ye, Y. Zhang, Q. Zhou, X. Niu, J. Wang, P. F. Li, D. W. Fu, Z. Wang, S. Gao, K. Yang, J. M. Liu, J. Li, Y. Yan and R. G. Xiong, An Organic-Inorganic Perovskite Ferroelectric with Large Piezoelectric Response, *Science*, 2017, **357**, 306–309.
166 W. Q. Liao, D. Zhao, Y. Y. Tang, Y. Zhang, P. F. Li, P. P. Shi, X. G. Chen, Y. M. You and R. G. Xiong, A Molecular Perovskite Solid Solution with Piezoelectricity Stronger than Lead Zirconate Titanate, *Science*, 2019, **363**, 1206–1210.
167 W. Li, Z. Wang, F. Deschler, S. Gao, R. H. Friend and A. K. Cheetham, Chemically Diverse and Multifunctional Hybrid Organic-Inorganic Perovskites, *Nat. Rev. Mater.*, 2017, **2**, 16099.

Published on 07 April 2020. Downloaded on 1/28/2026 4:44:51 PM.

This journal is © the Partner Organisations 2020